Submitted to Radiation Research

INACTIVATION OF HUMAN KIDNEY CELLS BY HIGH-ENERGY MONOENERGETIC HEAVY-ION BEAMS

Eleanor A. Blakely, Cornelius A. Tobias,
Tracy C. H. Yang, Karen C. Smith, and John T. Lyman

March 1979

Prepared for the U. S. Department of Energy
under Contract W-7405-ENG-48

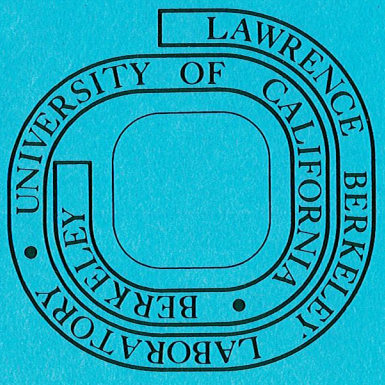

INACTIVATION OF HUMAN KIDNEY CELLS BY HIGH-ENERGY MONOENERGETIC HEAVY-ION BEAMS

Eleanor A. Blakely, Cornelius A. Tobias,
Tracy C. H. Yang, Karen C. Smith, and John T. Lyman

Biology and Medicine Division
Lawrence Berkeley Laboratory
University of California
Berkeley, California 94720

CONTENTS

	Page
List of Figures	iii
List of Tables	iv
Abstract	1
Introduction	3
Materials and Methods	7
Experimental Design	7
Cells and Culture Methods	7
Exposure Chamber and Gas Delivery Procedures	8
Irradiation Procedures	10
The Bevalac Facility	10
Heavy-Ion Dosimetry	11
Physical Characteristics of the Beams	21
X-Ray Dosimetry	24
Results	27
Survival Studies	27
Analytical Methods of Evaluating the Data	27
Inactivation Coefficients	41
Confidence Limits for the Inactivation Coefficients	44
RBE and OER Values	46
Confidence Limits for RBE and OER Calculation (Linear Quadratic Model)	52
Discussion	55
Comparison With Other Available Data	55
LET Dependence of Survival Parameters	56
LET Dependence of OER	62
Velocity and Charge Dependence of Lethal Effects	63
Conclusion	73
Acknowledgments	75
Notes	77
References	79

LIST OF FIGURES

		Page
1.	Schematic drawing of the exposure chamber and gas delivery procedure.	9
2.	Schematic drawing of the experimental alignment of equipment for the irradiation of cell monolayers under aerobic and hypoxic conditions at the Bevalac.	12
3.	Beam ranges studied with respect to the Bragg peak.	15
4.	Dose versus depth in water curves for the carbon, neon, and argon beams.	22
5.	X-ray (220-kVp) cell survival data for aerobic and hypoxic cell monolayers irradiated on glass and plastic surfaces.	25
6.	Heavy-ion cell survival data for aerobic and hypoxic cells irradiated in (A) the 400 MeV/amu carbon beam, (B) the 425 MeV/amu neon beam, and (C) the 570 MeV/amu argon beam.	28-30
7.	Error ellipses estimated for the $\underline{x}$ and $\underline{y}$ coefficients for fits of some of the neon data to the linear quadratic model.	45
8.	RBE versus survival level for the neon beam; aerobic and hypoxic cell data.	47
9.	OER and hypoxic RBE at 10% survival as a function of beam range for all three beams.	48
10.	Linear quadratic coefficients $\underline{x}$ and $\sqrt{\underline{y}}$ as a function of the dose-average mean LET_∞ for cell survival under aerobic conditions.	58
11.	Linear quadratic coefficients $\underline{x}$ and $\sqrt{\underline{y}}$ as a function of the dose-average mean LET_∞ for cell survival under hypoxic conditions.	59
12.	RBE values at 10% survival as a function of the dose-average mean LET_∞. Data are shown for aerobic and hypoxic cells irradiated with a carbon, neon, or argon beam.	60
13.	OER as a function of dose-average mean LET_∞ for carbon, neon, and argon beams; data from Blakely *et al.*, Barendsen, and Todd are compared.	64
14.	Cell inactivation cross section as a function of $1/\beta^2$ for aerobic and hypoxic cells.	69

LIST OF TABLES

		Page
I.	Physical characteristics of heavy-ion beams	
	A. Carbon Beam: 400 MeV/amu nominal energy (deflected at 4163 gauss)	16
	B. Neon Beam: 425 MeV/amu nominal energy (deflected at 4350 gauss)	17
	C. Argon Beam: 570 MeV/amu nominal energy (deflected at 5711 gauss)	18
II.	Dose and percent cell survival data for the different beam ranges studied with respect to the Bragg peak	
	A. Carbon Beam: Aerobic Cells	31
	B. Carbon Beam: Hypoxic Cells	32
	C. Neon Beam: Aerobic Cells	33
	D. Neon Beam: Hypoxic Cells	34
	E. Argon Beam: Aerobic Cells	35
	F. Argon Beam: Hypoxic Cells	37
III.	Best LSQ fits of $\underline{x}$ and $\underline{y}$ coefficients for the neon beam using three cell inactivation models (linear multitarget, linear quadratic, and repair saturation)	42
IV.	Best LSQ fits for the $\underline{x}$ and $\underline{y}$ coefficients for the carbon, neon, and argon beams using the linear quadratic model	43
V.	RBE and OER values for aerobic and hypoxic cells at 50% and 10% survival	
	A. Carbon Beam	49
	B. Neon Beam	50
	C. Argon Beam	51
VI.	Cell inactivation coefficients for equation (11)	68

ABSTRACT

Accelerated heavy particles are candidates for use in cancer therapy. The primary purpose of this investigation was to study the dose-effect relationships for asynchronous human kidney T-1 cells at various values of residual range for monoenergetic beams of carbon (400 MeV/amu), neon (425 MeV/amu), and argon (570 MeV/amu). The "track segment" method of exposure was used to minimize variations in the distribution of energy transfer events; secondary fragments produced by the particles in their passage through matter were, however, unavoidably included.

Cell survival was measured under aerobic and hypoxic conditions over a range of mean LET_∞ from 10 keV/μm to 600 keV/μm. Survival curves were characterized by an exponential and a nonlinear component. Using three current models for cellular inactivation, including the linear-quadratic model, we found that the linear inactivation coefficient increased dramatically with increasing particle charge and decreasing particle velocity. The quadratic coefficient was also found to be dependent on LET.

Dose and mean LET_∞ by themselves were not sufficient to characterize cellular responses. Three variables are needed: fluence; particle velocity; and particle charge or other equivalent quantities, such as dose, mean LET_∞, and charge. An analysis was made for the dependence of the inactivation cross section of the exponential survival term on the velocity parameter β. In an aerobic environment, the cross section varied as Z^4/β^4. In an hypoxic environment this cross section varied as $Z^4/\beta^{4.6}$. The total energy transfer is a function of Z^2/β^2 (neglecting a slowly varying logarithmic term) The radial distribution of transferred energy is a function of β^2 only, and is

independent of Z. Therefore, the $Z^{4.6}$ dependence is an indication of the importance of radial track structure.

The aerobic relative biological effectiveness values (RBE) measured at 10% survival (±95% C.I.) ranged from 1.1 ±0.2 to 2.6 ±0.4 for the carbon beam, 1.5 ±0.2 to 2.9 ±0.3 for the neon beam, and 2.1 ±0.4 to 2.7 ±0.3 for the argon beam. Hypoxic RBE values were greater than the aerobic RBEs for all of the beams, especially at low doses where survival is greater than 10%.

The maximum aerobic and hypoxic RBEs were obtained for the neon beam at an LET of approximately 140 keV/μm. The increase in RBE with LET appears to be independent of particle charge up to about 100 keV/μm; however, above 100 keV/μm, neon and argon RBE curves separate for the same mean LET_∞. The separation of the curves beyond 100 keV/μm may be a result of either the velocity dependence of the cell killing effect and/or due to the presence of greater fragmentation contributions in the argon beam.

The oxygen enhancement ratio (OER) at 10% survival drops from 2.9 ±0.3 at low LET to a limiting 1.2 ±0.1 in the Bragg peak of the neon and argon beams. The lowest OER measured for carbon was 1.6 ±0.5. For the argon beam the OER was lower than 2.0 for the last 5 cm of range and lower than 1.5 for the last 2 cm of range.

Although normal and tumor cells are known to have a range of biological properties, the RBE and OER results (and the LET, velocity, and charge dependence of these effects) presented here are basic to a fundamental understanding of the biological effects of charged particles. In addition, the data are relevant to future therapeutic uses of heavy ions.

INTRODUCTION

In this paper we present survival data on human kidney cells exposed to monoenergetic beams of high-energy carbon, neon, and argon ions accelerated at the Berkeley Bevalac. The experiments were carried out using particles with ranges up to 24 cm. The mean LET_∞ was varied between 10 keV/μm and 600 keV/μm under aerobic and hypoxic conditions. The dependence of cell survival parameters has been analyzed as a function of particle velocity (β) and atomic number (Z).

Following the early observation of differences in the effects of alpha and beta rays by Chambers and Russ (1), and Zirkle's introduction of the concept of biological effectiveness (2), there has been considerable confirmation that densely ionizing radiations are more effective in producing certain biological effects than sparsely ionizing radiations. Most of the early work was done on a variety of microorganisms, but more recently the validity of this conclusion has been demonstrated for mammalian systems with end points including cell lethality (3-9), division delay (10-12), chromosome aberrations (5, 13-15), carcinogenesis (16), cell transformation (17,18), point mutations (9, 19,20), and the production of double-strand scissions in mammalian cell DNA (21,22).

Studies with high-LET radiations have suggested that there are at least two different modes of action of ionizing radiations: one has a strong dependence on linear energy transfer (LET) with single-hit kinetics, and the other a weak dependence on LET with higher order kinetics. Using low-energy, accelerated heavy particles and the "track segment" method, it was demonstrated that at constant particle velocity the single-hit component of radiobiological effects strongly depends on the square of the atomic charge of the particles (3).

Thus, with respect to cell killing and barring saturation effects, particles with high Z are more effective than particles of low Z at the same velocity and the same dose. At high LET and high atomic number, the relative biological effectiveness (RBE), increases and the radiobiological oxygen effect decreases. For example, Barendsen et al. using helium ions (23), and Todd, using low-energy accelerated heavy ions (3), both demonstrated that the oxygen enhancement ratio (OER) for human kidney cells decreased to near unity at very high LET. However, these investigations covered only a limited range of particle velocities because of accelerator limitations.

Based on these early experimental results and theoretical considerations, Tobias and Todd (24) noted three characteristics of heavy-ion beams that made them potentially useful for clinical applications. First, the physical depth-dose distribution of heavy-ion beams is more advantageous than low-LET modalities for maximum effectiveness at depth with minimum entrance and exit dose. Second, stopping particles have an increased biological effectiveness compared to low-LET radiations. And third, the high ionization density of stopping particles reduces the oxygen effect, thereby decreasing the radioprotection of hypoxic cells.

Recent studies which established that high-LET radiations diminish cell age response and reduce fractionation effects have provided further support for using heavy ions for therapy (25,26). It is also likely that some aneuploid and hyperploid tumor cells are more sensitive to high-LET particle damage than are normal diploid cells (27,28). Some preliminary studies show that high-LET particles decrease the radioresistance of cells in spheroid culture compared to single-cell systems, a factor that might be due to altered environmental conditions or communication (29) between cells of the spheroid. Both of these effects might be operative for noncycling cells.

Several studies are underway at the Bevalac accelerator that use a distribution of kinetic energies produced by extending the Bragg peak of an accelerated heavy-ion beam for therapeutic purposes (30-33). Since the effects of secondary fragments are minimized in monoenergetic beams, it was desirable to conduct experiments in the more homogeneous particle fields that are available using the unmodified Bragg curves. In this paper, RBE and OER values based on detailed survival data are reported and evaluated as a function of particle range, rate of energy loss, and particle velocity for monoenergetic heavy-ion beams of carbon, neon, and argon. In addition, the physical dosimetric features of these beams have been characterized. The results of the pretherapeutic program generally justify and support earlier proposals made with respect to the potential clinical usefulness of heavy-ion beams (34).

MATERIALS AND METHODS

Experimental Design

Cells and Culture Methods

Human kidney T-1 cells[1] (35) were used because of the abundance of data on their responses to x rays, gamma rays, neutrons, and most importantly, low-energy accelerated heavy ions (3,23). The cells were cultured as monolayers in T flasks (Falcon Plastics) in Eagle's minimum essential medium with Earle's salts supplemented with 12.8% fetal bovine serum and the following antibiotics: potassium-penicillin G (0.04 g/l), streptomycin sulfate (0.04 g/l), gentamycin (0.09 g/l), and Fungizone (0.002 g/l). The flasks were maintained at 37°C in a humidified atmosphere of air with 5% CO_2. Stock cultures were transferred every three or four days so that the cells were maintained in exponential growth. Under these conditions, the mean population doubling time was about 22 hours. The concentration of glutamine was doubled for experimental cultures.

In preparation for each experiment, a 0.2-ml volume of 1.7×10^5 exponentially growing cells was plated in a circular area approximately 2 cm in diameter at the center of special glass petri dishes. After the cells attached to the bottom of the dish, they were covered with 1 ml of culture medium. The cells were irradiated between 12 and 24 hours after they were plated onto the glass dishes. After exposure, the cells were trypsinized, resuspended, counted, plated, and incubated at 37°C for 10 to 12 days. Colony-forming ability was scored by staining the cultures with 1.0% methylene blue, and clones containing at least 100 cells were scored as survivors. Colony counts on four or more plastic petri dishes were averaged for each data point. Eight

or more dishes were used for control and high-dose samples. Colony counts per dish were usually in the 50 to 300 range, and plating efficiencies usually were 60% to 70%.

Exposure Chamber and Gas Delivery Procedure

The dose along the Bragg ionization curve near the peak varies greatly with small changes in absorber thickness, even changes as small as 0.01 g/cm^2. Thus, in order to position the cells accurately in the beam at various residual-range values, the cells were grown as monolayers on a support of uniform thickness. Special sealed aluminum and glass chambers[2] with fitted glass petri dishes (35 mm in diameter and a bottom surface 0.02-cm thick) were built to facilitate control of the interior gas milieu (see Figure 1).

Each chamber was equipped with a gas pressure gauge. For the actual exposure, each chamber (loaded with cells on the petri dish) was filled with the appropriate gas mixture and sealed somewhat higher than ambient pressure (25 to 38 cm of water). Small gas leaks not sufficient to appreciably change the internal positive pressure would therefore force nitrogen to leak out rather than air to leak in.

The glass petri dishes were secured in the chamber with a teflon-type plastic (viton) o-ring, and a set of brass and aluminum rings that were threaded for the chamber. The medium was completely aspirated from each dish, and 0.3 ml of fresh medium was added just before loading to buffer and preserve the moist condition of the cells during gassing.

The internal volume of the petri dish within the gassing chamber was approximately 12.5 cc. The chamber was attached to a coiled, copper tube from a manifold that the gas passed through after being humidified (see Figure 1).

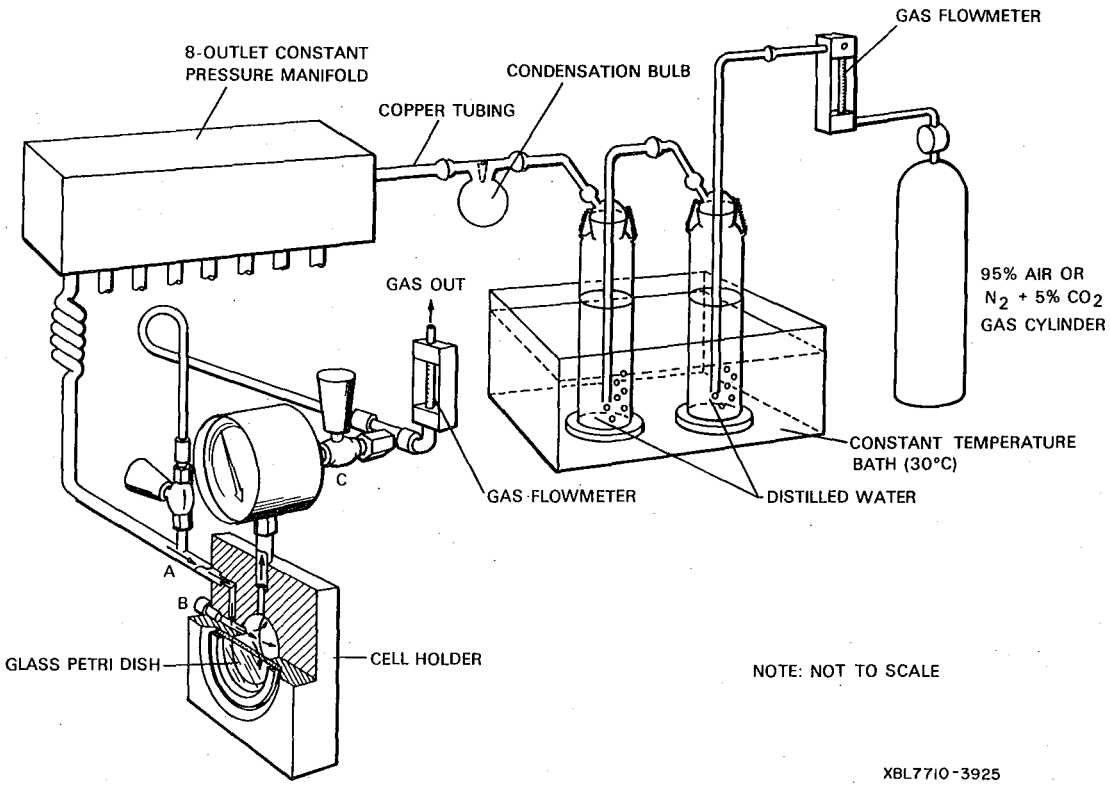

Figure 1:

Exposure chamber and gas delivery procedure. Humidified gas (95% air + 5% CO_2 for aerobic exposures and 95% nitrogen + 5% CO_2 for hypoxic exposures) is flushed through OER chambers by means of a manifold. The chamber is sealed at exhaust valve C and inlet valve B with a slight positive pressure (25 to 38 cm of water) just prior to irradiation. The chamber is designed with a by-pass loop (A-C) which is used for pretesting the integrity of the chamber.

The gas delivery apparatus was flushed for at least an hour with nitrogen gas before the chambers were attached. During gassing the chambers were in a horizontal position, and shaken frequently and gently so that the cells were continually covered with a thin film of medium.

The gas mixtures used in the experiments were either 95% air with 5% CO_2, or 95% nitrogen with 5% CO_2 containing less than 2 ppm (parts per million) O_2. Gases were obtained from the Pacific Oxygen Co. (Oakland, CA).

The flow rate of the gas through the chamber was approximately 160 to 240 cc/min, and the cells were gassed for 20 to 30 min. This represented a gas volume turnover per minute of 10 to 20 times the internal volume of the dish in each holder. The nitrogen samples were irradiated immediately after gassing; air samples were not held for more than 30 min after gassing and were usually irradiated well within this time interval.

Chambers used for hypoxic exposures were screened for oxygen leaks with the couloximeter trace oxygen monitor (Chemical Sensor Development Co., Minneapolis, MN). A reading in ppm of oxygen by volume can be made with a sensitivity of approximately 10 ppm. Corrections were made for background readings, a fuel-cell yield of 0.85, and a gas dilution factor implicit in the flushing method used to analyze the oxygen concentration in the nitrogen gassing chambers. A mean corrected oxygen concentration of 64 ±29 ppm by volume was obtained for the fourteen nitrogen chambers, each fitted with a different, randomly selected, glass petri dish.

Irradiation Procedures

The Bevalac Facility

The Bevalac (36) is a high-energy heavy-ion accelerator complex created in 1974 by joining the Superhilac (a heavy-ion linear accelerator) and the

Bevatron (a proton synchrotron). The particles were accelerated to an extraction energy of 400 MeV/amu for carbon, about 425 MeV/amu for neon, and about 570 MeV/amu for argon. Fully stripped $^{12}_{6}C$, $^{20}_{10}Ne$, and $^{40}_{18}A$ ions were utilized.

For our experiments the beam emerged from a thin mylar window into biomedical cave 2, and then traveled in air to the exposure bench. The alignment of equipment on the optical bench is diagrammed in Figure 2. Instrumentation and computer operation for dosimetry of the Bevalac beams were initially developed by J. T. Lyman, and later extended by J. Howard.[3]

Heavy-Ion Dosimetry

The experiments reported here were conducted over a three-year period. For the earlier experiments, angular divergence of the beam was adjusted with quadrapole steering and focusing magnets. Later, lead scattering foils (1.3 g-cm^{-2} for the carbon and neon beams, and 0.9 g-cm^{-2} for the argon beam) were inserted in the beam upstream from the last set of quadrapole and steering magnets.[4] The multiple scattering in these foils produced an angular divergence of the beam, and also produced some secondary fragments. Standard settings for the focusing magnets were used to focus the unscattered beam near the location of entry into the exposure room. The beam diameter was usually 3 to 5 cm, and there was about a 6% dose variation across the cell monolayer. The doses measured by the central collectors assured us that the beam distribution was uniform.

In all the experiments beam uniformity was checked with a pair of multiwire proportional chambers that provided a visual display of the integrated beam intensity distribution projected in the vertical and horizontal directions.

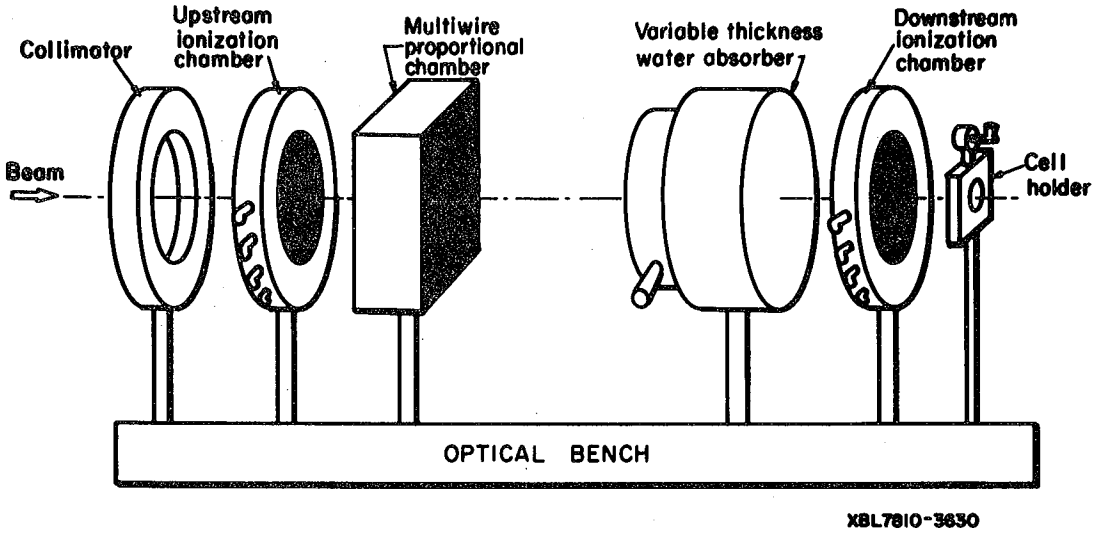

Figure 2:

Experimental alignment of equipment for irradiation of cell monolayers under aerobic and hypoxic conditions at the Bevalac. The cells mounted in the cell holder on an optical bench are exposed to heavy-ion beams. The beam enters from the left through a collimator. A multiproportional chamber gives information on the localization and size of the beam, and beam range is modulated by a remote controlled variable thickness water absorber. The Bragg ratio is measured as the ratio of ionization measured in the second ion chamber to that measured in the monitor ion chamber. The central collector of the second ion chamber (1-cm diameter) is used to measure the dose.

Beam centering and the intensity distribution were also verified in each experiment by checking the uniformity of an exposed polaroid film. The radial distribution of ionization in the beam was measured in an ionization chamber which has six concentric rings 1, 3, 5, 7, 9, and 11 cm in diameter. This chamber was located immediately upstream of the biological samples.

The instrumentation used for beam centering and dosimetry was developed by Lyman et al. at the Lawrence Berkeley Laboratory (37,38). The general dosimetry followed principles first used by Tobias et al. (39) and later discussed by Raju et al. (40). Parallel-plate ionization chambers (see Figure 2) were used with a circular collecting electrode. One chamber was mounted in the upstream position, intercepting the beam as it arrived at the exposure bench. The second chamber was mounted downstream, behind the variable water absorber and immediately before the cell sample holder. The ionization chambers were continually flushed with dry nitrogen gas. W, the average energy to make one ion pair in the nitrogen gas, was assumed to be equal to 34.9 eV. This value was derived from data for alpha particles in nitrogen gas (41), and agrees with recent work by Lyman (42).

The same value of W was used for the entire Bragg curve, although for nearly stopping particles W should be significantly higher than the value quoted (43). We are also aware that columnar recombination might occur. There was good agreement between Fricke dosimetry, parallel plate ion chambers, and EGG ion chambers for dose measurements in the "plateau." We believe that the "plateau" measurements are within 5% and the "peak" within 15% of absolute dose measurements. A comparison of argon beam depth-dose measurements in our laboratory with those done independently later by Goodman and Colvett (44) showed excellent agreement.

The cell sample was positioned directly behind the downstream ion chamber. Corrections were made for the dose drop off in the air space between the ion chamber and the sample. Prior to some experiments a calibrated 1-cc tissue equivalent thimble chamber (EGG Model No. IC-17A) was positioned at the exact location the sample would occupy during the experiment for a cross reference check on the measured absorbed dose. The residual range values indicated in Figure 3 and Tables I A, B, C represent the actual positions where cell samples were exposed. A variable thickness water absorber (see Figure 2) was used to obtain each position along the track.

The monolayer samples were irradiated in the vertical position perpendicular to the beam. In this position, most of the medium drained to the bottom of the dish, leaving a thin layer to cover the cells, however, no dose correction was made for the residual medium. All exposures were completed at room temperature. The dose rate was usually 100 to 300 rad/min, and most exposures were completed in less than 10 minutes. The doses were administered at 15 pulses per minute, and each pulse was a few tenths of a second long with a complex and variable time structure. The downstream ionization chamber was electronically triggered with the PDP 11/45 computer to cut off the beam at the requested dose. For the positions near the Bragg peak, it was necessary to correct the dose measured in the downstream ion chamber in order to account for the extra absorption due to the air space, sample holder glass, and the foils of the ion chamber. To do this, we measured the relative stopping power of glass to water. The dose corrections were read from the Bragg curves measured on the same day, however, no interface dose correction was made (see below).

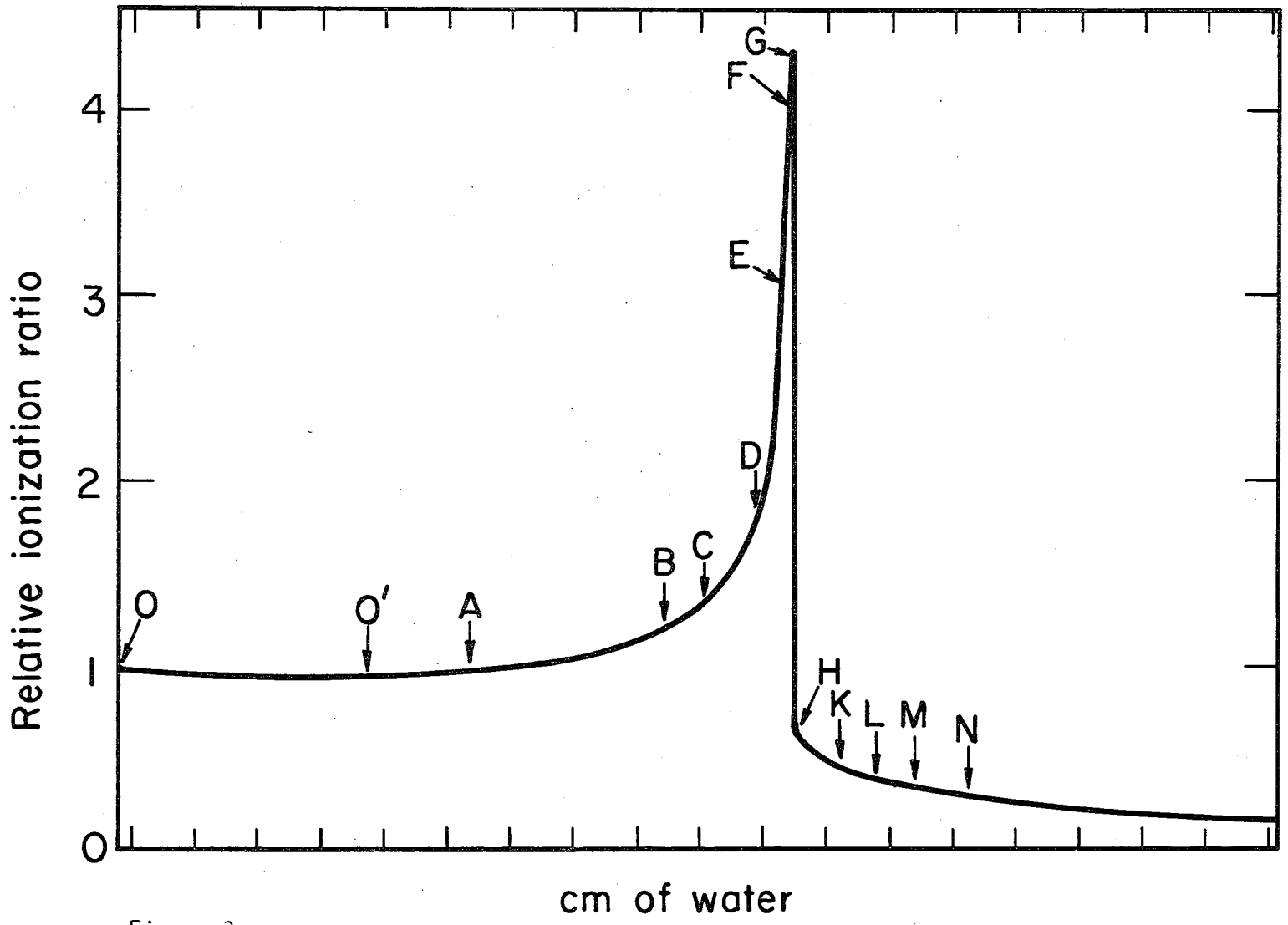

Figure 3:

XBL777-3591a

Beam ranges studied with respect to the Bragg peak. See residual ranges listed in Table I.

TABLE IA. CARBON: 400 MeV/amu Nominal Energy (Deflected at 4163 Gauss)

I	II	III	IV	V	VI	VII	VIII	IX	X
Position	Residual Range[1] ($cm\ H_2O$)	Bragg Ionization Ratio[2] ($I_{corr.}$)	Bragg Ratio Calculated for Primary $^{12}_{6}C$ Beam Only	Percent of Ionization Due to Fragments Calculated[3] (%)	Flux Density Calculated for Primary $^{12}_{6}C$ Beam[4]	Residual Energy Calculated for $^{12}_{6}C$ Particles[5] (MeV/amu)	Mean LET Calculated for $^{12}_{6}C$ Particles[6] (keV/μm)	Mean LET of Fragments[7] (keV/μm)	Mean LET of Beam[8] (keV/μm)
0	25.2	1.00	1	< 1 to 3	1	380	11	7	11
0'	9.0	0.97	0.78	20	0.62	206	16	8	13
A	6.8	1.03	0.77	25	0.48	175	18	10	16
B	2.4	1.35	0.97	28	0.40	98	27	13	23
C	1.2	1.61	1.20	25	0.38	67	36	14	30
D	0.54	2.0	1.58	21	0.37	47	47	14.5	40
E	0.29	2.39	1.99	17	0.35	33	87	14.8	65
F	0.14	3.07	2.53	18	0.32	24	118	15	85
G	0.04	3.37	2.84	16	0.28	16	144	16	124
Peak	0	3.42	2.86	16	0.24	12	178	16	123
H	0.2	0.45	---	100	---	---	---	15	15
K	1.0	0.41	---	100	---	---	---	15	15
L	2.0	0.36	---	100	---	---	---	14	14
M	3.0	0.32	---	100	---	---	---	13	13

TABLE IB. NEON: 425 MeV/amu Nominal Energy (Deflected at 4350 Gauss)

I	II	III	IV	V	VI	VII	VIII	IX	X
Position	Residual Range[1]	Bragg Ionization Ratio[2]	Bragg Ratio Calculated for Primary $^{20}_{10}Ne$ Beam Only	Percent of Ionization Due to Fragments Calculated[3]	Flux Density Calculated for Primary $^{20}_{10}Ne$ Beam[4]	Residual Energy Calculated for $^{20}_{10}Ne$ Particles[5]	Mean LET Calculated for $^{20}_{10}Ne$ Particles[6]	Mean LET of Fragments[7]	Mean LET of Beam[8]
	(cm H_2O)	($^{I}_{corr.}$)		(%)		(MeV/amu)	(keV/μm)	(keV/μm)	(keV/μm)
0	16.1	1.00	1.00	<1 to 5	1.00	370	32	26	32
0'	---	---	---	---	---	---	---	---	---
A	6.8	1.03	0.86	17	0.66	235	41	26	38
B	2.4	1.30	0.99	24	0.52	129	60	35	54
C	1.2	1.58	1.20	24	0.485	88	80	42	71
D	0.54	1.97	1.48	25	0.464	57	118	48	100
E	0.29	2.50	1.96	22	0.456	42	164	54	139
F	0.14	3.07	2.52	22	0.446	31	284	58	234
G	0.04	4.23	3.53	22	0.426	21	520	63	419
Peak	0	4.56	3.60	16	0.358	16	620	65	531
H	-0.2	0.58	---	100	---	---	---	58	22
K	-1.0	0.44	---	100	---	---	---	54	18
L	-2.0	0.32	---	100	---	---	---	52	13
N	-4.0	0.19	---	100	---	---	---	54	11

TABLE IC. ARGON: 570 MeV/amu Nominal Energy (Deflected at 5711 Gauss)

I	II	III	IV	V	VI	VII	VIII	IX	X
Position	Residual Range[1]	Bragg Ionization Ratio[2]	Bragg Ratio Calculated for Primary $^{40}_{18}A$ Beam Only	Percent Ionization Due to Fragments Calculated[3]	Flux Density Calculated for Primary $^{40}_{6}A$ Beam[4]	Residual Energy Calculated for $^{40}_{18}A$ Particles[5]	Mean LET Calculated for $^{40}_{18}A$ Particles[6]	Mean LET of Fragments[7]	Mean LET of Beam[8]
	(cm H_2O)	($I_{corr.}$)		(%)		(MeV/amu)	(keV/μm)	(keV/μm)	(keV/μm)
0	15	1	1	<1 to 8	1 to 0.92	505	85	38	81
0'	---	---	---	---	---	---	---	---	---
A	6.8	0.96	0.65	30	0.51	304	110	45	91
B	2.4	1.20	0.66	45	0.35	165	164	60	117
C	1.2	1.49	0.79	48	0.32	112	209	74	144
D	0.54	1.87	1.0	49	0.30	72	277	89	184
E	0.29	2.18	1.22	48	0.29	54	370	109	245
F	0.14	2.46	1.5	47	0.28	39	521	110	328
G	0.04	2.91	2.08	41	0.27	22	1009	110	640
Peak	0	3.56	2.64	26	0.24	17	1040	100	714
H	-0.2	0.81	---	100	---	---	---	95	95
K	-1.0	0.49	---	100	---	---	---	69	69
L	-2.0	0.28	---	100	---	---	---	52	52
M	-3.0	0.19	---	100	---	---	---	32	32

FOOTNOTES TO TABLE I (A,B, and C)

[1]Equivalent water absorber distance between position and experimentally obtained Bragg peaks; negative numbers are used beyond the peak. The numbers include a correction (0.06 cm) for absorption by ion chamber and sample holder.

[2]Ratio of ionization at the sample position to ionization at the sample position with no absorber:

$$I_{corr.} = \alpha I;\ I = \frac{\frac{I_\alpha}{I_u}\ \text{absorber}}{\frac{I_\alpha}{I_u}\ \text{no absorber}}$$

I_α is the ionization measured downstream of the water absorber, 1-cm diameter collector. I_u is the ionization measured in the upstream ionization chamber large collector. "α" is a correction factor to take into account the change in Bragg ratio due to absorption in downstream chamber walls, air, and sample holder. Values for α range from 1.0 to 1.24.

[3]The initial contamination of the beam with fragments is very small when no absorbers are interposed, and it is larger when lead scatterers are used.

[4]Relative to the beam emerging from the accelerator (1.0).

[5]The energy is a mean value and is based on flux distribution calculations. In addition to the energies quoted in the table, we used neon (400 MeV/amu) and argon (500 MeV/amu) normal initial energies. The only values that show significant change are in the first line.

[6]Dose average mean LET_{∞}.

[7]Calculated for fragments with strong forward momentum only. Twelve fragment species were estimated; their yield was adjusted to produce a fragment dose curve in agreement with the experimental data. For the neon and argon beams, the proton, helium, neutron, and "exotic" fragments (such as pions) were left out. Together these produce less than 3% of the dose, therefore their use would distort the average LET values.

[8]Dose averages; hydrogen, helium, and exotic fragments have been omitted. The low-LET fragments were included for the portion beyond the range, however, because these represent a significant portion of the dose.

Physical Characterization of the Beams

Ionization measurements for the beams are presented in Figure 4. Measurements from several experiments yielded consistent information. The minor variations we encountered resulted in slight shifts of the Bragg ionization peak, and were due to fluctuations in primary beam energy. These fluctuations in the primary beam energy were a result of variations in the magnetic field values in the main acceleration ring at which the pulsed beam was deflected over a several hour period. There were also changes in the composition of the beam fragments from run to run because of different absorber configurations used upstream from the samples. The energy of the available neon beam varied from run to run (from 400 to 430 MeV/amu). The argon experiments were conducted at 500 and 570 MeV/amu. All of the carbon experiments were done at 400 MeV/amu. In a given run, the range of the particles was observed to shift about 0.05 cm (or 0.3%) in the worst case.

The open circles on the Bragg curves shown in Figure 4 are normalized Bragg ionization ratios. The experimental points were compared to a calculated Bragg curve (solid line, Figure 4). The mean rate of energy loss was based on an approximation of the Bohr Bethe formula as described by Steward (45). The results were compared to a compilation by Richard-Serre (46), however, an accurate experimental confirmation of the range energy relationship from 50 to 1000 MeV/amu is needed. Schimmerling et al. confirmed the range energy results for N^{7+}, Ne^{10+}, and A^{18+} within a few percent (47).

For total fragmentation cross section we used a general formula initially derived by Bradt and Peters from cosmic ray data (48); the cross section was made energy dependent corresponding to recent experimental work indicating increases in overall fragmentation cross sections below 200 MeV/amu. There

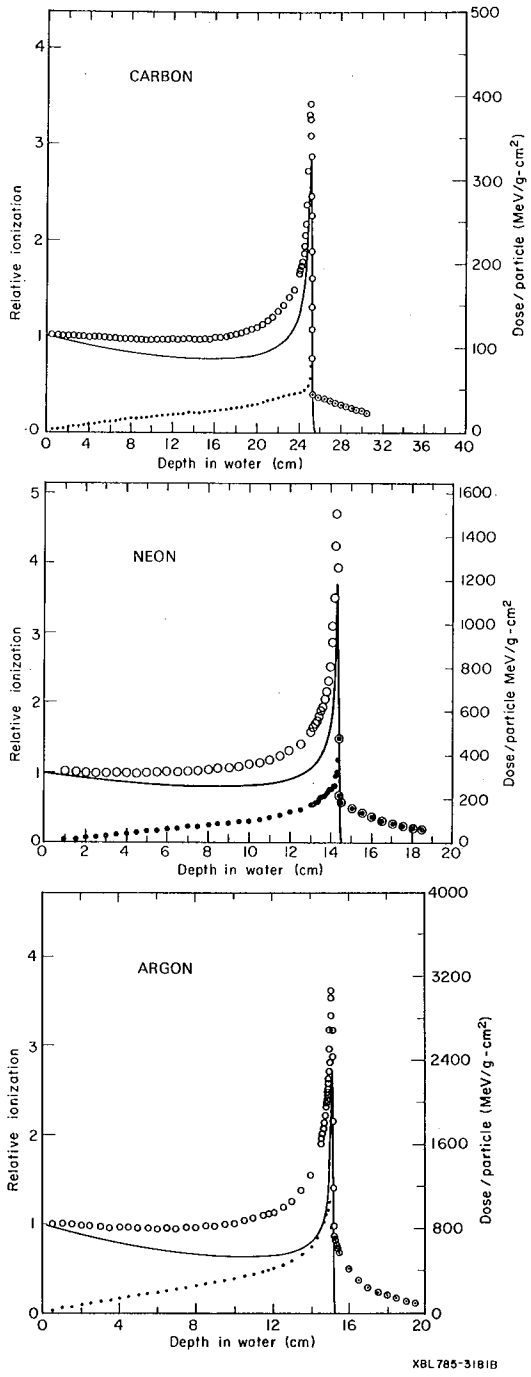

Figure 4:

Dose vs depth curves in water. Actual normalized ionization ratios measured (O). Calculated ionization contributions from secondary fragments (●). Calculated Bragg curve (—), see description in text.

is active current experimental work on the fragmentation process. Data from Heckman et al. (49), Maccabbee and Ritter (50), Schimmerling et al. (51), and Chatterjee et al. (52) have helped in estimating the dose contributions from fragmentation.

The computed Bragg curve is plotted with a continuous line in Figure 4. The difference between the measured Bragg curve (open circles) and the computed Bragg curve is due to fragmentation; this difference is shown by solid points in Figure 4. Beyond the particle range, the fragmentation effects (circles with solid points) are measured directly. The contribution from fragments in the monoenergetic beam increases from a small value at the plateau to a maximum a few millimeters upstream from the Bragg peak.

We estimate that the error of the calculated "fragment" dose just upstream from the Bragg peak might be as much as 20% of the values given. The total fragment dose is always less than the dose that would have been delivered by the unfragmented parent particle. Fragmentation increases with the atomic number of the primary particle, therefore, fragmentation effects are greater for argon (up to 49%) and less for neon (about 25%). The carbon beam is not strictly comparable to the neon and argon beams because it has a much longer range.

In Tables IA, IB, and IC, we have listed the most important physical parameters of the beams used in the current experiments for the positions where cells were exposed in monolayers. The "mean LET_∞" in these figures is "dose average LET" a quantity calculated from our present understanding of the energy transfer and fragmentation processes. Curtis has published a method of calculating median LET_∞ (53). The mean values independently calculated by us for 0.05-cm segments of track are given in Table I. For some of the

experimental points the mean LET_∞ values represent averages over a wide spectrum of LETs, and must be considered estimates.

There are some central collisions of the primary beam with the atoms of the biological material that can produce numerous atomic fragments, mostly of low atomic number, emitted at various angles to the beam. There are also recoil target nuclei and the fragments from these. We estimate the overall dose contributions from these are small, a few percent at most; however, at some future time it might be important to assess the local effects of multi-pronged nucleon stars in heavy-ion irradiated tissue. The effects of wide angle scattering and target fragmentation are not dealt with explicitly in this paper.

X-Ray Dosimetry

X-irradiation of the cells was performed with a Philips x-ray unit (Type 11645) operated at 220 kVp and 15 mA with filtration of 0.25-mm Cu and 1-mm Al, and HVL of 0.75-mm Cu. The dose rate was usually 270 rad/min, as measured with a calibrated Victoreen condenser 250 R-meter at a target distance of 24 cm. Fricke and thermoluminescent dosimetry were used to confirm Victoreen dose measurements; the Fricke data[5] agreed within 2% and the TLD data[6] within 5%. The exact gas delivery method and geometry used for the heavy-ion exposures were duplicated for the x-ray experiments. Experiments were done with cells attached in monolayers to both glass and plastic substrates in 2-cm diameter areas.

Glass was used to support the cell monolayers and to construct the chambers because plastics hold large quantities of oxygen and release it

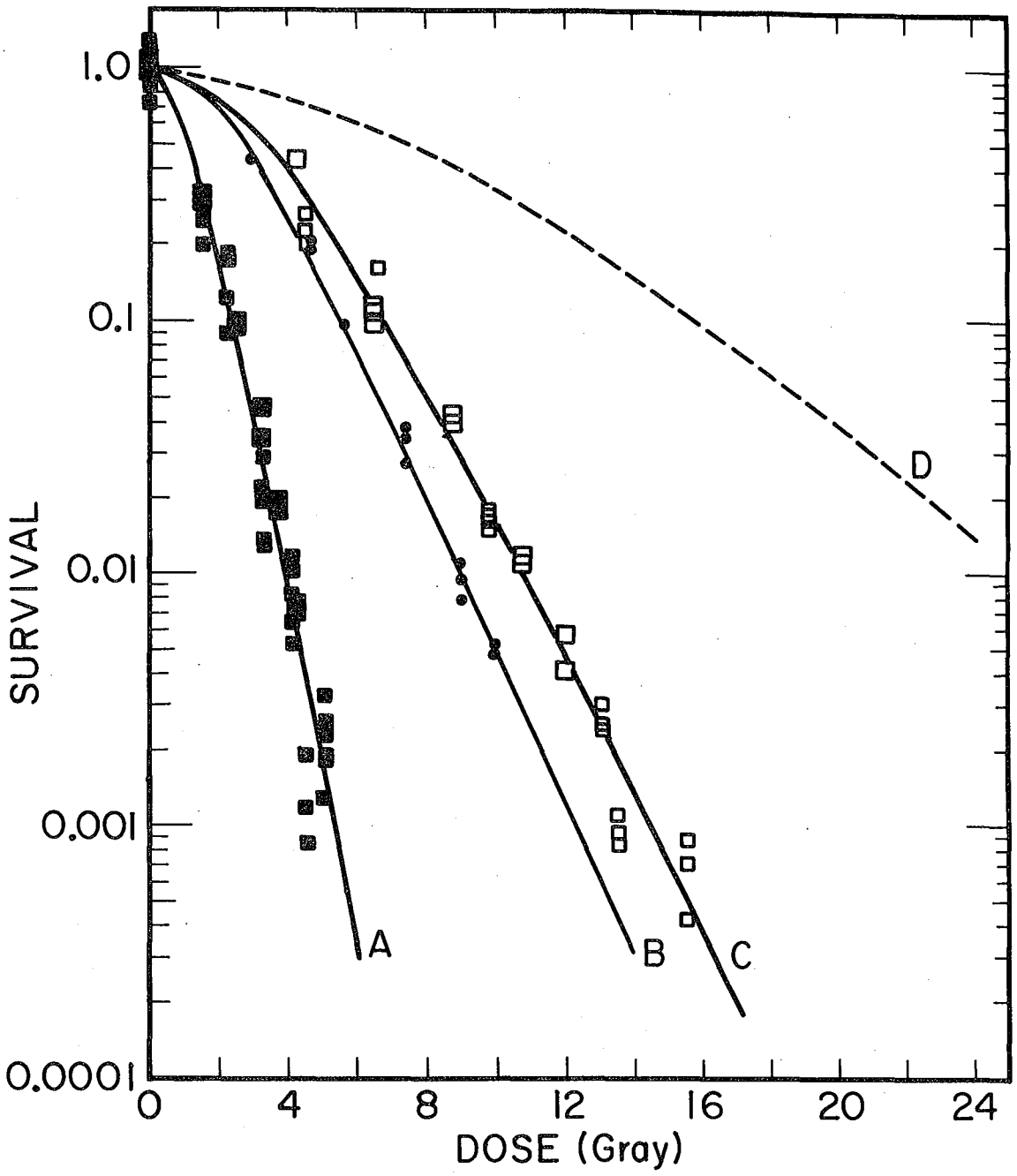

Figure 5:

XBL7710-3934 A

220-kVp x-ray cell survival data:

(■) aerobic survival for cells irradiated on glass,

(□) hypoxic survival for cells irradiated on glass,

(●) aerobic survival for cells irradiated on plastic,

(—) hypoxic survival for cells irradiated on plastic (calculated).

slowly by diffusion (54). At a given measured dose, the x-ray survival measured for cells irradiated on glass was considerably less than for cells irradiated on plastic because of scattered secondary electrons. The correction factor for the additional dose from scattered electrons is strongly dependent on the energy and HVL of the x rays used (55,56). A two-fold difference in survival between cells irradiated on plastic versus cells irradiated on glass was measured under our x-ray exposure conditions. A derived hypoxic survival curve for T-1 cells irradiated on a plastic substrate was constructed from comparisons of the aerobic and hypoxic survival curves from cells irradiated on glass (see Figure 5). We assumed that the OER was not influenced by differences between glass and plastic. Kidney-cell monolayers grown on glass and on plastic petri dishes were also exposed to 400 MeV/amu neon beams. No statistically significant differences for survival on glass or plastic were detected. This agrees with the theoretical idea that essentially all ionization in heavy-ion beams comes from ion pairs, and delta rays produced by the primary beam particles--and not from scattered secondary electrons. Therefore, no interface dose corrections were made for heavy-ion doses.

RESULTS

Survival Studies

Aerobic and hypoxic cell survival curves for the carbon, neon, and argon beams studied are shown in composite Figures 6A, 6B, 6C. In most cases, results have been pooled from two to four separate experiments. The continuous lines in the figure represent least-square fits to the linear-quadratic model. Survival data for each beam (aerobic and hypoxic) can be found in Tables IIA through IIF.

X-ray survival curves from cells irradiated on glass and on plastic surfaces in air, and on glass in hypoxic conditions are shown in Figure 5. On glass, an OER of 2.9 ±0.3 was obtained at the 10% survival level. Figure 5 also shows the derived hypoxic survival curve for x rays on plastic (see Methods section).

Analytical Methods for Evaluating the Data

Three different forms of survival equations were used to evaluate our data. The first one of these represents a combination of a single-hit process with a multitarget expression (57-59). The survival "S" as a function of the dose (D) in this linear multitarget (LMT) model is:

$$S_{LMT} = c\left\{1 - \left[1 - \exp(-qD)\right]^{m}\right\} \exp(-pD) \qquad (1)$$

There are four adjustable variables: p, q, m, and c. The single hit, or "linear" term is characterized by an inactivation constant p, whereas the multitarget process depends on the extrapolation number m and the inactivation constant q. The parameter c, which takes care of the "plating efficiency"

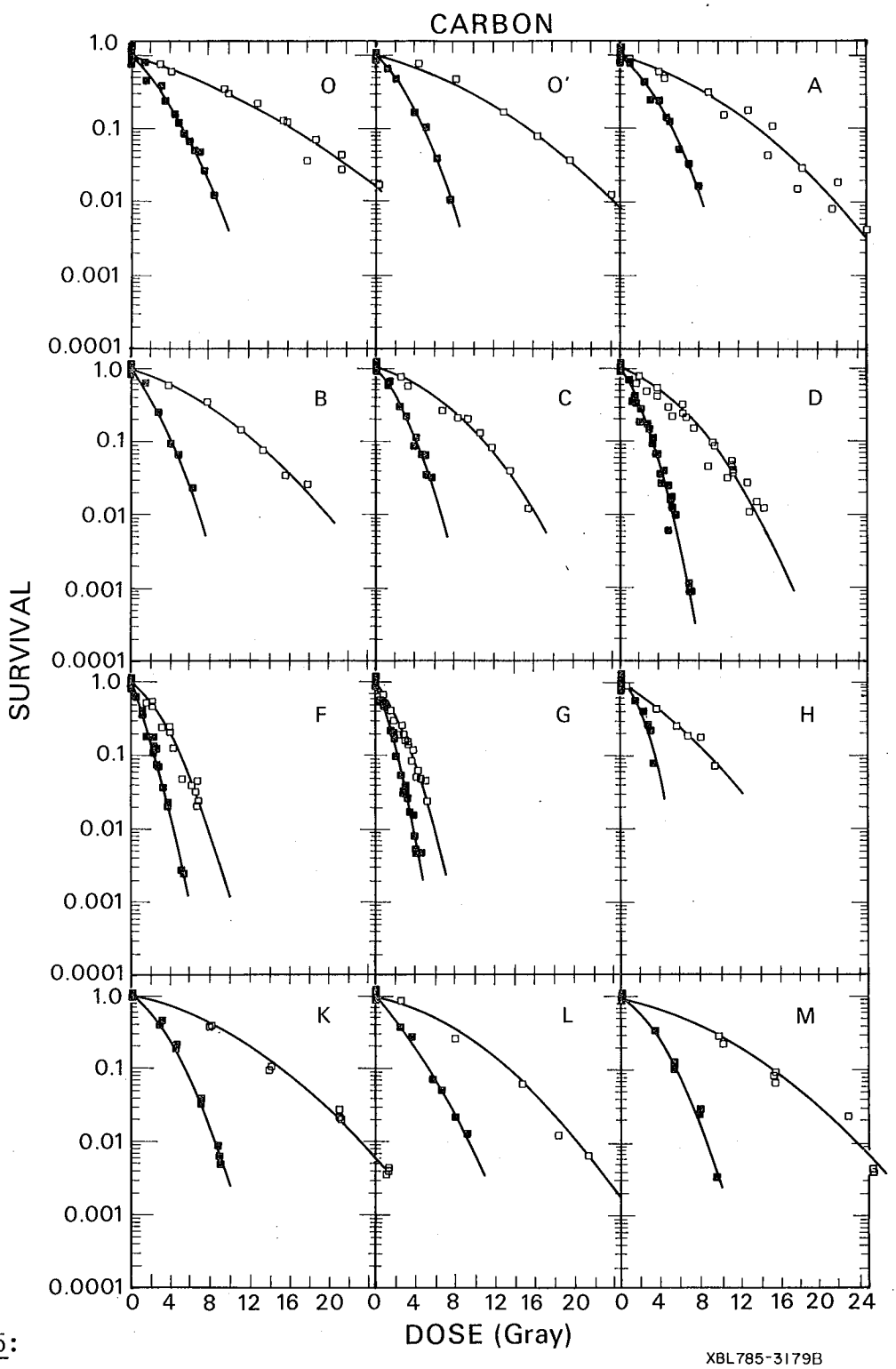

Figure 6:

Heavy-ion cell survival data: aerobic (■), hypoxic (□). The alphabetical letter in the upper right of each set of curves designates the range studied as described in Figure 3 and Table I. Date are from one to four experiments for each set of curves:

6A = 400 MeV/amu carbon beam

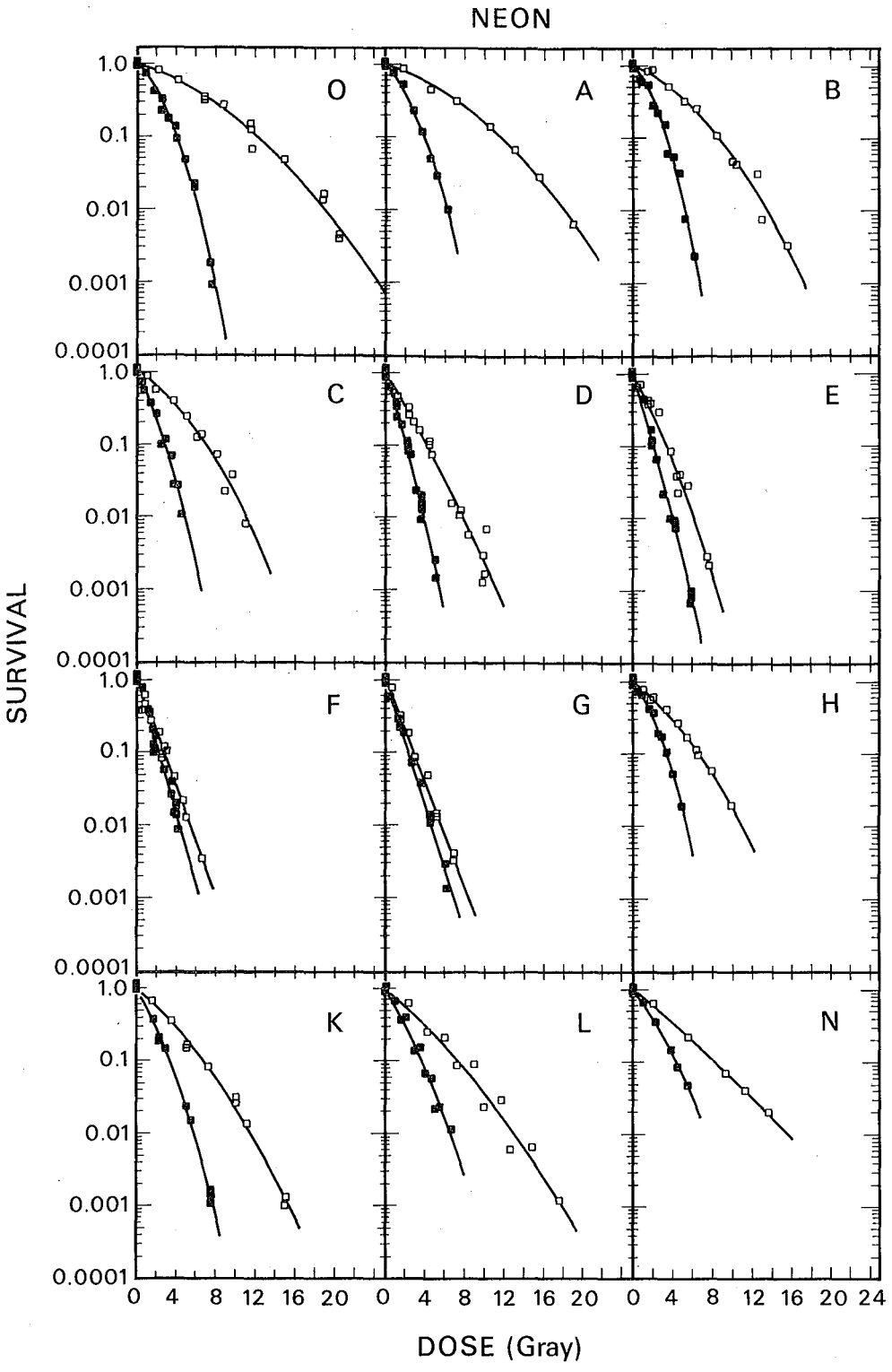

6B = 425 MeV/amu neon beam

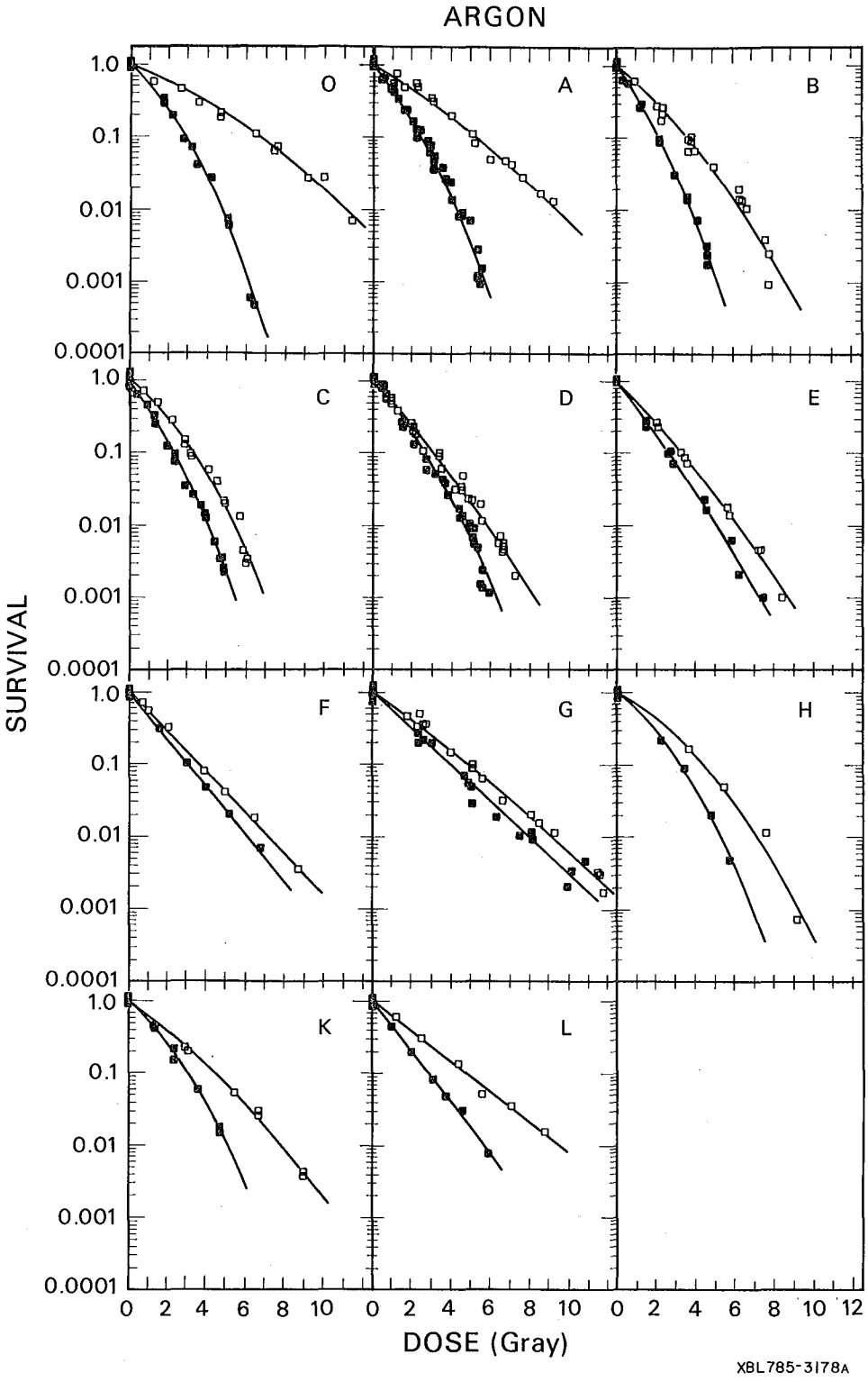

6C = 570 MeV/amu argon beam

TABLE IIA. Carbon Beam: Aerobic Cells

O		X		A		B		C		D		F		G		H		K		L		M	
Rad	% S	Rad	% S	Rad	% S	Rad	% S	Rad	% S	Rad	% S	Rad	% S	Rad	% S	Rad	% S	Rad	% S	Rad	% S	Rad	% S	Rad	% S
0	92.0	0	88.0	0	92.0	0	100	0	96.0	0	102	0	100	0	93.0	0	95.0	0	109	0	107	0	105	0	106
0	103	0	109	0	103	0	103	0	85.0	0	98.0	0	103	0	95.0	0	105	0	132	0	92.0	0	88.0	0	92.0
0	100	0	109	0	100	0	104	0	121	0	100	0	104	0	95.0	0	94.0	0	86.0	0	107	0	115	0	106
0	105	0	94.0	0	105	0	93.0	0	98.0	0	100	0	93.0	0	117	0	106	0	73.0	0	94.0	0	92.0	0	96.0
150	78.7	120	66.5	100	75.5	140	63.3	142	59.9	157	43.6	92.4	67.9	114	42.1	55.0	56.7	53.0	91.8	287	44.8	250	36.1	543	10.1
320	38.7	219	47.4	250	42.5	280	24.9	142	63.8	161	34.2	205	28.4	111	37.9	143	21.9	148	56.7	293	47.5	360	26.3	337	34.2
450	15.9	400	16.5	400	23.3	400	9.38	305	21.0	160	40.6	329	11.6	240	12.6	209	9.83	233	41.2	277	39.2	580	6.85	337	35.0
550	8.41	520	10.1	500	12.1	480	6.70	406	10.9	296	14.6	370	7.10	218	11.1	253	5.40	265	27.8	450	21.8	660	4.92	551	12.1
650	5.05	630	3.91	600	5.04	620	2.26	506	6.36	276	17.8	442	4.02	218	13.3	297	3.33	297	21.7	443	19.1	800	2.08	541	12.1
750	2.66	770	1.06	700	3.29					287	17.6	493	2.52	240	7.40	352	1.74	329	7.98	441	19.4	920	1.24	544	12.4
										298	15.6			353	2.24	0	1.00			705	4.05			810	2.89
										528	1.72			366	2.03	232	19.4			699	3.28			792	2.77
										528	1.24			520	0.238	238	18.6			694	3.98			792	2.54
										510	1.54			499	0.273	407	0.810			892	0.498			975	0.339
										694	0.115					394	1.55			881	0.620			972	0.333
										713	0.0915					467	0.471			871	0.860			967	0.328
										692	0.0916					401	0.523								
																402	0.464								
0	87.0			0	109			0	90.0	0	95.0	0	105	0	95.0	0	86.0								
0	103			0	132			0	109	0	103	0	88.0	0	105	0	92.0								
0	122			0	86.0			0	92.0	0	96.0	0	115	0	94.0	0	127								
0	88.0			0	73.0			0	99.0	0	106	0	92.0	0	106	0	95.0								
150	46.7			100	85.2			0	110	103	36.0	205	18.5	55.2	60.6	85.0	47.5								
350	24.5			300	23.5			122	52.3	328	9.68	349	6.91	144	17.5	82.9	54.0								
500	12.3			480	13.6			244	28.5	411	3.55	411	2.73	210	17.8	172	20.9								
600	6.97			600	4.96			386	8.24	514	1.54	493	0.612	265	6.67	183	17.2								
700	4.90			700	3.08			457	6.52			565	1.01	320	3.54	285	3.93								
850	1.26			800	1.57			518	3.26					376	2.27	314	3.95								
								567	3.01							320	2.67								

TABLE II B. Carbon Beam: Hypoxic Cells

O		X		A		B		C		D		F		G		H		K		L		M	
Rad	% S	Rad	% S	Rad	% S	Rad	% S	Rad	% S	Rad	% S	Rad	% S	Rad	% S	Rad	% S	Rad	% S	Rad	% S	Rad	% S	Rad	% S
0	96.0	0	98.0	0	96.0	0	83.0	0	112	0	93.0	0	83.0	0	78.0	0	94.0	0	106	0	117	0	106	0	104	0	100
0	97.0	0	111	0	97.0	0	109	0	91.0	0	104	0	109	0	111	0	109	0	93.0	0	103	0	91.0	0	119	0	107
0	99.0	0	98.0	0	99.0	0	94.0	0	97.0	0	102	0	94.0	0	100	0	97.0	0	113	0	86.0	0	101	0	82.0	0	93.0
0	108	0	93.0	0	108	0	114	254	70.8	0	101	0	114	0	111	131	37.5	0	88.0	0	94.0	0	102	0	95.0	0	100
420	59.6	450	76.8	450	50.0	390	57.5	260	77.5	361	51.7	185	74.7	211	46.1	185	29.2	339	14.6	360	43.3	794	36.0	260	83.7	1031	21.2
950	34.1	820	46.3	900	31.9	780	33.5	254	72.8	365	41.5	493	28.3	207	51.8	266	24.9	336	13.6	562	25.2	790	35.5	800	25.4	1040	21.3
1300	22.0	1310	16.9	1300	18.5	1120	13.9	254	75.5	641	31.2	750	14.5	396	20.2	287	18.8	369	8.18	678	18.6	803	37.2	1480	5.87	998	26.3
1600	12.1	1650	7.94	1550	10.9	1340	7.31	843	20.7	651	23.0	965	8.56	388	23.8	425	5.05	514	4.34	806	17.2	1411	10.1	1840	1.18	1558	8.97
1900	6.99	1986	3.66	1850	2.97	1570	3.40	1059	12.3	676	20.4	1149	3.59	672	4.30	437	5.93	477	4.61	954	7.10	1400	10.5	2150	0.625	1548	7.88
2150	4.22	2400	1.29	2200	1.85	1800	2.52			1135	5.08	1284	2.63	645	2.98	575	0.791	631	0.956			1392	9.35	2500	0.259	1561	6.24
										1128	4.60			926	0.207	577	0.841	637	0.702			2093	2.62			2295	2.31
										1518	0.392			967	0.162			161	39.7			2110	2.04			2300	2.26
										1521	0.425			389	19.7							2093	2.10			2298	2.16
														381	21.4							2592	0.310			2565	0.383
														661	1.94							2610	0.360			2555	0.413
																						2612	0.388			2543	0.425

0	141	0	117	0	97.0	0	102	0	104	0	103	0	103		
0	86.0	0	103	0	113	0	112	0	119	0	97.0	0	97.0		
0	73.0	0	86.0	0	95.0	0	89.0	0	82.0	0	107	0	107		
0	100	0	94.0	0	95.0	0	97.0	0	95.0	0	93.0	0	93.0		
300	75.4	400	60.4	325	55.7	267	45.1	154	60.4	144	50.2	87.9	65.8		
1000	30.3	1050	15.3	671	25.6	945	9.22	534	21.0	309	22.9	297	15.5		
1550	12.5	1500	4.44	935	19.9	1150	3.90	894	4.36	420	12.0	385	11.2		
1800	3.69	1800	1.54	1178	8.09	1383	1.43	1089	3.06	519	4.51	451	4.58		
2150	2.74	2150	0.811	1361	3.84			1314	1.04	608	3.73	528	2.29		
2550	1.72	2500	0.435	1544	1.18			1458	1.15	682	2.24				

TABLE IIC. Neon Beam: Aerobic Cells

O		A		B		C		D		E		F		G		H		K		L		N	
Rad	% S	Rad	% S	Rad	% S	Rad	% S	Rad	% S	Rad	% S	Rad	% S	Rad	% S	Rad	% S	Rad	% S	Rad	% S	Rad	% S
0	92.3	0	114	0	87.1	0	106	0	91.6	0	91.6	0	110	0	97.9	0	112	0	103	0	106	0	100
0	102	0	96.4	0	111	0	104	0	104	0	104	0	90.0	0	97.9	0	92.2	0	96.7	0	103	0	95.0
0	109	0	91.5	0	109	0	93.5	0	97.7	0	97.7	0	88.9	0	109	0	103	0	104	0	95.4	0	101
0	97.1	0	97.5	0	92.9	0	96.8	0	107	0	107	0	111	0	95.4	0	93.5	0	91.6	0	95.1	0	104
252	21.5	80.0	75.0	60.2	65.3	50.4	71.9	117	38.7	193	10.2	166	19.5	129	29.1	48.8	73.2	0	1.04	100	68.5	100	64.1
251	30.6	180	49.8	151	54.9	141	36.3	113	25.3	200	11.8	167	12.4	136	22.4	97.5	65.2	222	20.2	200	39.9	220	35.3
392	13.1	290	22.4	251	22.2	202	25.2	113	34.9	200	10.3	174	9.65	263	7.49	156	40.6	223	19.9	350	15.2	380	14.7
389	12.8	380	11.6	326	15.2	282	11.4	213	11.1	431	.749	395	1.60	262	7.12	205	37.4	223	18.7	470	5.80	450	8.56
581	2.09	450	4.92	412	5.62	353	6.69	222	9.63	426	.862	355	3.85	455	1.42	251	18.5	501	2.31	553	2.26	550	4.69
585	1.90	520	2.84	472	3.32	423	2.71	219	8.40	418	.942	386	1.45	452	1.09	292	16.9	499	2.23	660	1.15		
769	.086	628	.987					363	2.04	595	.0998	400	1.37	610	.296			502	2.17				
745	.171							362	1.31	591	.0676	399	1.95	615	.135			747	.155				
								359	.922	603	.0809	668	.382					752	.104				
								500	.257			659	.300					750	.132				
								504	.146			645	.258										
0	114			0	94.6	0	102	0	83.4	0	83.4	0	87.7	0	87.7	0	87.7	0	94.6	0	100		
0	96.4			0	106	0	105	0	111	0	111	0	120	0	120	0	120	0	106	0	95.0		
0	91.5			0	101	0	104	0	106	0	106	0	100	0	100	0	100	0	101	0	101		
0	97.5			0	97.9	0	88.7	0	99.1	0	99.1	0	92.6	0	92.6	0	92.6	0	97.9	0	104		
100	69.8			80.3	58.6	70.5	54.3	41.3	64.2	43.5	65.0	45.1	74.3	42.4	59.4	87.2	62.3	170	35.7	150	37.4		
180	39.5			201	27.5	242	9.55	103	40.6	109	44.2	113	38.1	182	19.1	330	10.5	298	13.8	290	13.9		
320	16.5			351	6.21	373	2.76	165	19.7	185	16.6	192	16.6	351	3.85	397	5.18	548	1.43	400	6.73		
400	8.74			522	.759	453	1.05	248	7.29	250	6.52	271	5.56			484	1.93			510	2.19		
480	4.57			622	.231			310	2.37	316	2.16	350	2.58										
								362	1.55	381	1.04	417	.853										

TABLE IID. Neon Beam: Hypoxic Cells

O		A		B		C		D		E		F		G		H		K		L		N	
Rad	% S	Rad	% S	Rad	% S	Rad	% S	Rad	% S	Rad	% S	Rad	% S	Rad	% S	Rad	% S	Rad	% S	Rad	% S	Rad	% S
0	96.2	0	101	0	105	0	97.4	0	89.4	0	86.6	0	94.1	0	95.9	0	94.5	0	110	0	104	0	110
0	99.6	0	90.3	0	106	0	92.7	0	106	0	113	0	106	0	104	0	109	0	89.9	0	108	0	103
0	104	0	100	0	87.2	0	114	0	83.7	0	105	0	111	0	95.0	0	103	0	103	0	84.6	0	95.5
682	33.5	0	108	0	102	0	95.9	0	121	0	94.8	0	89.2	0	105	0	93.4	0	97.3	0	103	0	91.8
680	31.5	180	84.9	151	83.5	101	85.8	236	25.6	149	37.4	146	26.6	148	29.0	97.5	74.7	504	14.8	230	62.7	200	62.9
1159	12.1	450	43.6	351	50.3	376	38.8	233	32.9	149	42.3	79	42.7	146	31.7	195	60.6	500	14.3	594	21.0	546	22.2
1166	6.52	718	29.8	638	25.6	501	23.8	435	11.1	156	38.5	85	37.0	295	8.58	338	40.5	503	16.1	892	8.99	930	7.01
1884	1.57	1050	13.6	850	10.8	649	13.1	434	10.3	457	3.74	51	38.0	290	7.44	452	26.4	997	2.89	1168	2.94	1130	4.11
1877	1.32	1300	6.57	1041	4.40	806	7.09	748	1.08	453	3.72	271	11.5	520	1.45	545	16.2	999	2.44	1476	.662	1360	1.99
2054	.434	1550	2.83	1252	3.24	967	3.65	757	1.22	456	2.28	78	59.6	511	1.37	639	11.3	998	2.44	1748	.121		
2050	.377	1900	.633					972	.298	758	.305	259	8.36	687	.411			1504	.126				
								1011	.0682	754	.294	253	9.23	675	.332			1501	.0964				
								975	.124	771	.224	661	.335										
												508	1.23										
												505	1.24										
0	101			0	88.3	0	102	0	105	0	105	0	103	0	103	0	103	0	88.3	0	110		
0	90.3			0	104	0	100	0	88.7	0	88.7	0	92.1	0	92.1	0	92.1	0	104	0	103		
0	100			0	91.4	0	102	0	98.1	0	98.1	0	118	0	118	0	118	0	91.4	0	95.5		
0	108			0	116	0	95.2	0	108	0	108	0	86.2	0	86.2	0	86.2	0	116	0	91.8		
220	77.6			201	87.7	181	55.3	111	46.0	65.3	72.1	56.5	73.3	60.5	78.8	175	56.8	150	63.5	420	25.8		
420	57.4			512	32.4	604	12.2	278	20.4	163	40.8	135	34.7	230	18.7	649	9.76	350	34.1	720	8.56		
879	26.7			997	4.84	886	2.20	339	15.9	272	29.6	214	18.3	424	4.90	795	5.80	720	7.78	1000	2.34		
1150	14.3			1305	.746	1098	.791	461	7.44	381	8.57	305	10.1			988	1.90	1114	1.28	1250	.606		
1490	4.66			1566	.328			665	1.53	479	3.85	384	4.49										
								829	.553	566	2.84	474	2.14										
								997	.161														

TABLE IIE. Argon Beam: Aerobic Cells

O		A		B		C		D	
Rad	% S	Rad	% S	Rad	% S	Rad	% S	Rad	% S
0	99.0	0	104	0	99.0	0	101	0	98.0
0	106	0	112	0	101	0	76.0	0	108
0	103	0	90.0	0	108	0	93.0	0	106
0	92.0	0	94.0	0	92.0	0	130	0	88.0
178	35.4	216	12.4	128	26.7	135	23.9	153	25.4
180	30.1	204	15.4	133	29.3	130	33.0	151	28.3
346	3.96	230	9.22	131	29.2	132	30.9	265	8.48
345	3.92	319	5.26	228	9.01	236	9.65	271	8.48
503	0.731	316	4.43	228	8.32	237	8.96	457	1.34
510	0.595	313	3.35	228	9.31	387	1.41	451	1.35
641	0.0487	406	1.30	373	1.56	395	1.22	560	0.138
622	0.0602	433	0.750	375	1.42	475	0.351	552	0.150
		459	0.737	376	1.38	372	1.79		
		548	0.0887	474	0.173	482	0.248		
		535	0.1125	471	0.234	468	0.335		
		533	0.109	33	59.5	483	0.216		
						236	7.55		
0	109	0	110	0	102	0	89.0	0	93.0
0	88.0	0	90.0	0	100	0	86.0	0	107
0	103	104	40.0	0	98.0	0	109	148	27.1
80	103	538	0.263	60.2	54.8	0	116	277	5.68
220	19.7	555	0.140	124	26.6	40.8	63.0	443	1.26
280	9.34			308	2.92	91.8	45.1	591	0.116
320	7.18			417	0.692	194	12.0		
320	6.78			469	0.300	286	3.45		
420	2.51					326	2.61		
520	1.58					439	0.578		

TABLE IIE. contd.

E		F		G		H		K		L	
Rad	% S	Rad	% S	Rad	% S	Rad	% S	Rad	% S	Rad	% S
0	94.0	0	100	0	117	0	85.0	0	88.0	0	99.0
0	106	0	84.0	0	99.0	0	104	0	103	0	84.0
292	7.18	0	103	0	94.0	0	111	0	115	0	103
743	0.100	0	113	0	90.0	223	21.6	0	94.0	0	114
0	92.0	74.9	72.2	231	19.7	348	8.92	146	42.6	100	45.6
0	103	161	31.6	255	21.4	475	2.03	139	44.5	200	20.3
0	98.0	300	10.6	231	25.3	572	0.474	238	21.1	310	8.29
0	107	396	4.74	485	5.23			242	15.6	380	4.82
155	28.2	514	2.03	468	6.50			362	5.81	460	3.02
152	23.6	674	0.692	813	1.11			364	5.52	590	0.787
275	9.96			813	0.914			471	1.56		
276	10.3			1084	0.442			472	1.79		
450	2.21			1017	0.324						
459	1.65										
585	0.629										
623	0.213										

0	100
180	45.3
298	19.3
502	4.89
630	1.80
0	124
0	104
0	72.0
234	26.1
507	2.86
751	0.981
995	0.200

TABLE IIF. Argon Beam: Hypoxic Cells

O		A		B		C		D	
Rad	% S	Rad	% S	Rad	% S	Rad	% S	Rad	% S
0	97.0	0	98.0	0	97.0	0	99.0	0	111
0	101	0	92.0	0	94.0	0	98.0	0	100
0	97.0	0	112	0	96.0	0	85.0	0	94.0
0	105	0	98.0	0	113	0	103	0	95.0
470	19.8	125	76.4	240	26.5	0	115	201	24.0
467	18.0	160	50.3	245	20.5	284	15.7	198	255
763	6.97	228	53.1	238	17.4	284	13.4	336	10.0
744	6.02	308	33.0	409	6.46	284	15.4	335	9.15
1297	0.405	398	21.0	392	10.0	319	9.38	547	1.98
1297	0.314	520	8.53	392	8.73	317	9.54	546	1.98
1799	0.0051	602	5.00	632	1.38	320	9.96	714	0.143
1812	0.0091	673	4.77	647	1.31	490	2.15	729	0.138
651	10.2	768	2.83	630	1.90	483	2.23		
1143	0.681	856	1.68	783	0.0874	486	2.08		
1530	0.038	916	1.36	785	0.234	606	0.346		
						595	0.316		
						587	0.463		
0	106	0	94.0	0	95.0	0	94.0	0	100
0	108	0	98.0	0	104	0	98.0	211	18.6
0	99.0	0	101	0	101	0	101	349	5.96
0	99.0	0	107	101	58.4	0	107	548	1.16
0	88.0	100	58.2	208	26.7	71.4	73.6	716	0.0867
120	55.8	220	59.1	373	8.91	143	51.4		
260	44.4	300	35.4	372	6.06	224	28.5		
360	27.7	510	11.5	502	3.84	408	5.87		
920	2.59	710	4.26	671	1.03	449	4.24		
1000	2.64	920	1.37	764	0.365	561	1.38		
1240	0.715								

TABLE IIF. contd.

E		F		G		H		K		L	
Rad	% S	Rad	% S	Rad	% S	Rad	% S	Rad	% S	Rad	% S
0	101	0	111	0	98.0	0	100	0	108	0	111
0	101	0	97.0	0	107	0	91.0	0	100	0	97.0
0	96.0	0	87.0	0	97.0	0	109	0	88.0	0	87.0
0	102	0	105	0	98.0	366	16.7	0	104	0	105
212	22.7	96.3	55.1	257	35.8	543	5.08	305	20.4	120	62.8
348	8.66	203	30.7	263	36.7	752	1.14	294	22.7	250	31.8
203	26.5	385	7.96	510	10.1	916	0.0743	545	5.28	440	13.8
358	7.28	492	4.09	511	8.92			546	5.26	560	5.38
348	8.67	642	1.79	928	1.15			670	2.57	710	3.71
575	1.42	867	0.367	1159	0.298			670	3.02	880	1.55
563	1.75			1147	0.333			898	0.424		
728	0.455			0	101			902	0.381		
721	0.447			0	116						
0	100			0	83.0						
333	9.92			240	50.1						
842	0.0993			559	6.33						
				849	1.54						
				1179	0.171						
				0	98.0						
				0	102						
				227	33.6						
				397	14.5						
				663	3.14						
				811	1.99						

and adjusts the origin of the curve to 100% survival, is needed for the statistical treatment. In our application of this model we arbitrarily held m equal to 6, a value that was obtained from the analysis of x-ray curves and was also used by Todd (3). We have shown earlier that the value of p increases at high LET (3,60).

The second expression is the linear quadratic model (LQ), which was first used for cell survival experiments by Jacobson (61) and Sinclair (62). Various authors proposed terms that are proportional to D^2 for the production of chromosome aberrations, and these have been analyzed by Neary (63). A theoretical foundation was given by Kellerer and Rossi (64,65). An additional interpretation of the linear quadratic model was given in molecular terms by Chadwick and Leenhouts (66,67):

$$S_{LQ} = c \exp (-xD - yD^2) . \qquad (2)$$

Here x, the linear inactivation coefficient, has the same role as p in the LMT model; y is a constant relating to the quadratic term; and c normalizes the curve at the origin.

The third model has an entirely different basis from the first two. Following Haynes' early suggestions relating to the effects of ultraviolet radiation (68), it was assumed that the shoulder of survival curves is caused by molecular DNA repair processes. We chose the form suggested by Green and Burki (69) called the "repair saturation" model (RS).

$$S_{RS} = \frac{(r + 1)}{r + \exp (gD)} . \qquad (3)$$

Here g is an inactivation constant and r relates to the probability of repair. The role of c is the same as in the LQ and LMT models. The RS model assumes that there is a finite quantity of repair enzyme present which limits the amount of repair possible. The above formula has not been rigorously derived for ionizing radiation. An earlier derivation by Ginsberg and Jaggers for ultraviolet rays (70) brought in additional assumptions.

The initial slope of the survival curves at low doses is given by:

$$-p \simeq -x \simeq \frac{-g}{r + 1} \tag{4}$$

At large doses the LMT and RS models converge to

$$me^{-(p + q)D} \simeq (r + 1)e^{-gD}, \tag{5}$$

so that the extrapolation number is $m \simeq r + 1$ and $g = p + q$. The LQ model has no "final" slope; the curve continues to bend at high doses.

Computer assisted curve fitting was done with each of the models to determine which model best fitted the data, and how the constants in these models varied as a function of residual range and residual energy of the particle beams. The logarithm of averaged colony counts was used to fit the logarithm of the appropriate survival function. The approximation was done with three independent variables: two related to the functional form of the survival equation and the third represented the intercept of the survival curve at zero dose (c).

Each of the survival forms were nonlinear functions of the dose, and a grid search was used for the nonlinear programs. The LQ model was also

studied by linear matrix.[7] In order to do this, least-square approximations were performed on the logarithm of the survival data, which provided appropriate weighting.

Having determined the best values of $\underline{x}$, $\underline{y}$, and $\underline{c}$, the survival curves were normalized to $\underline{c} = 1$ and plotted (Figure 6). The percentage error in $\underline{c}$ was usually much smaller than that of $\underline{x}$ or $\underline{y}$. The 95% confidence limits for $\underline{x}$ and $\underline{y}$ coefficients were estimated from a calculated error matrix based on Chi-square tables. $\underline{X}$ and $\underline{y}$ values represent the intersections of an error ellipse with the $\underline{x}$ and $\underline{y}$ axis (see below) (71).

In order to obtain the dose dependence of derived quantites such as RBE and OER, we proceeded by obtaining least-squares fits to the survival data using the linear-quadratic model, and then calculating the appropriate ratios using the best fits (see below).

Inactivation Coefficients

Table III shows the best fit cellular inactivation coefficients for the neon beam for all three models. The number of experimental points are given for each position on the Bragg curve (95% confidence limits based on Student's t values). For the same number of degrees of freedom, the statistical treatments used show that the fit of all three models is equivocal.

The best fit $\underline{x}$ and $\underline{y}$ values (with 95% confidence limits) for the linear quadratic model for the three beams are given in Table IV. The $\underline{x}$ parameter is an indicator of the linear component of survival, and is dominant at low doses. In all cases, this component reaches a maximum near the Bragg peak. The $\underline{y}$ parameter, which dominates at very high doses, can be readily estimated for the plateau, but it is difficult to estimate near the Bragg peak because

TABLE III. Best LSQ Fits of x and y for Neon Beam with Three Models of Cell Inactivation

		Linear Multitarget		Linear Quadratic		Repair Saturation	
Aerobic Position	n	p ($\times 10^{-3}$)	q ($\times 10^{-3}$) m = 6	x ($\times 10^{-3}$)	y ($\cdot 10^{-6}$)	g ($\cdot 10^{-3}$	r ($\cdot 10^{0}$)
0	21	2.7 ±1.2	7.9 ±1.2	2.4 ±0.7	8.2 ±1.7	11.4 ±1.2	10.2 ±9.8
A	11	3.1 ±0.4	7.1 ±0.4	3.3 ±0.4	6.7 ±0.8	9.9 ±0.4	4.0 ±0.8
B	19	3.8 ±1.4	8.2 ±1.6	3.4 ±0.6	8.0 ±1.7	12.4 ±1.4	6.2 ±6.0
C	18	7.1 ±1.6	5.9 ±2.0	5.7 ±0.5	6.3 ±1.3	11.2 ±1.6	1.6 ±1.8
D	23	9.9 ±1.2	6.0 ±1.8	9.5 ±1.2	6.0 ±2.8	13.8 ±1.2	1.1 ±1.0
E	23	11.0 ±0.8	3.5 ±1.4	10.4 ±0.7	2.7 ±1.5	12.4 ±0.8	0.4 ±0.6
F	22	10.3 ±1.6	2.7 ±4.0	10.2 ±0.7	0.8 ±3.7	10.5 ±1.6	0.0 ±0.0
G	19	10.0 ±1.0	0.0 ±0.2	10.0 ±0.9	0.0 ±0.2	10.0 ±1.0	0.0 ±0.0
H	18	4.5 ±0.8	7.0 ±1.0	3.9 ±0.7	8.8 ±1.8	10.7 ±1.0	2.8 ±1.4
K	21	6.2 ±0.4	4.8 ±0.6	5.5 ±0.4	4.4 ±0.6	9.9 ±0.8	1.6 ±1.0
L	18	5.7 ±1.0	3.7 ±1.4	5.4 ±0.8	2.5 ±1.6	7.9 ±1.0	0.8 ±1.0
N	9	4.6 ±0.2	3.6 ±0.4	4.1 ±0.2	2.7 ±0.4	6.6 ±0.2	0.8 ±0.2
Hypoxic Position							
0	20	1.1 ±0.4	2.3 ±0.4	1.0 ±0.3	0.8 ±0.2	3.4 ±0.4	5.6 ±4.8
A	11	1.0 ±0.2	2.5 ±0.2	1.0 ±0.1	0.8 ±0.1	3.4 ±0.2	4.2 ±1.8
B	19	0.8 ±0.6	3.9 ±0.6	1.6 ±0.4	1.0 ±0.4	4.8 ±0.6	5.3 ±4.6
C	18	2.1 ±0.6	3.6 ±0.8	2.1 ±0.2	1.4 ±0.2	5.5 ±0.8	3.6 ±3.0
D	24	5.5 ±1.0	2.0 ±1.6	5.3 ±0.9	0.7 ±1.0	7.1 ±0.6	1.1 ±1.0
E	23	5.7 ±1.0	4.3 ±1.2	7.0 ±0.9	1.1 ±1.3	8.8 ±1.0	1.3 ±1.4
F	25	8.2 ±1.2	2.1 ±2.8	8.2 ±1.0	0.5 ±2.1	8.5 ±1.2	0.0 ±0.0
G	19	7.9 ±0.8	2.1 ±1.8	7.9 ±0.7	0.5 ±1.3	8.4 ±0.8	0.1 ±0.4
H	18	2.6 ±0.2	3.1 ±0.4	2.3 ±0.3	1.7 ±0.4	4.9 ±0.8	1.8 ±0.8
K	20	3.1 ±0.4	2.4 ±0.4	2.6 ±0.3	1.2 ±0.2	5.0 ±0.4	1.8 ±1.8
L	18	2.8 ±0.6	2.0 ±0.8	2.6 ±0.5	0.7 ±0.4	4.3 ±0.6	1.6 ±2.4
N	9	2.8 ±0.2	1.0 ±0.4	2.6 ±0.1	0.2 ±0.1	3.1 ±0.2	0.3 ±1.8

TABLE IV. Best LSQ Fits for x and y for Carbon, Neon, and Argon Beams Using the Linear Quadratic Model

	CARBON			NEON			ARGON		
Aerobic Position	n	x ($\times 10^{-3}$)	y ($\times 10^{-6}$)	n	x ($\times 10^{-3}$)	y ($\times 10^{-6}$)	n	x ($\times 10^{-3}$)	y ($\times 10^{-6}$)
0	20	2.8 ±0.4	2.6 ±0.7	21	2.4 ±0.7	8.2 ±1.2	22	5.2 ±1.4	9.8 ±2.8
0'	10	2.5 ±0.4	4.4 ±0.6	--	--------	--------	--	--------	--------
A	20	2.2 ±0.6	4.0 ±0.8	11	3.3 ±0.4	6.7 ±0.8	21	7.3 ±1.0	8.9 ±2.1
B	10	3.8 ±0.5	4.0 ±0.8	10	3.4 ±0.6	8.0 ±1.7	24	7.9 ±0.7	9.9 ±1.6
C	20	3.3 ±0.8	5.3 ±1.7	10	5.7 ±0.5	6.3 ±1.3	27	8.3 ±0.5	8.0 ±1.1
D	45	3.9 ±1.2	8.8 ±1.9	15	9.5 ±1.2	6.0 ±2.8	21	7.4 ±1.1	8.7 ±2.2
E	--	--------	--------	23	10.4 ±0.7	2.7 ±1.5	16	7.9 ±0.6	2.1 ±1.1
F	24	8.1 ±1.0	6.9 ±2.4	22	10.2 ±0.7	0.8 ±3.7	10	7.5 ±0.4	0.2 ±0.7
G	29	7.4 ±1.7	11.0 ±0.5	19	10.0 ±0.9	0.0 ±0.2	25	5.8 ±0.7	0.01 ±0.02
H	10	1.2 ±1.9	15.4 ±0.7	18	3.9 ±0.7	8.8 ±1.8	7	4.5 ±0.6	8.1 ±1.3
K	16	2.2 ±0.2	3.8 ±0.4	21	5.5 ±0.4	4.4 ±0.6	12	4.9 ±0.5	8.1 ±1.3
L	10	3.4 ±0.3	1.6 ±0.4	18	5.4 ±0.8	2.5 ±1.6	10	7.6 ±0.5	0.9 ±1.0
M	16	1.9 ±0.4	3.8 ±0.5	--	--------	--------	--	--------	--------
N	--	--------	--------	9	4.1 ±0.2	2.7 ±0.4	--	--------	--------
Hypoxic Position									
0	20	0.9 ±0.2	0.3 ±0.1	20	1.0 ±0.3	0.8 ±0.2	26	2.3 ±0.3	1.7 ±0.2
0'	10	0.8 ±0.1	0.5 ±0.1	--	--------	--------	--	--------	--------
A	20	0.8 ±0.4	0.6 ±0.2	11	1.0 ±0.1	0.8 ±0.1	25	3.6 ±0.4	1.4 ±0.6
B	10	1.0 ±0.2	0.7 ±0.1	10	1.6 ±0.4	1.0 ±0.4	25	4.8 ±1.0	3.6 ±1.4
C	19	0.7 ±0.3	1.3 ±0.2	10	2.1 ±0.2	1.4 ±0.2	27	4.3 ±0.5	7.8 ±0.9
D	41	0.9 ±0.5	1.8 ±0.4	13	5.3 ±0.9	0.7 ±1.0	17	5.2 ±0.9	5.4 ±1.5
E	--	--------	--------	13	7.0 ±0.9	1.1 ±1.3	16	6.1 ±0.3	2.1 ±0.5
F	25	2.3 ±0.7	4.6 ±0.8	25	8.2 ±1.0	0.5 ±2.1	10	6.2 ±0.3	0.3 ±0.4
G	32	3.4 ±0.9	7.1 ±1.6	19	7.9 ±0.7	0.5 ±1.3	24	4.4 ±0.3	0.7 ±0.4
H	9	1.9 ±0.4	0.7 ±0.5	18	2.3 ±0.3	1.7 ±0.4	7	3.1 ±0.6	4.8 ±0.9
K	16	0.6 ±0.1	0.6 ±0.1	20	2.6 ±0.3	1.2 ±0.2	12	4.2 ±0.3	2.0 ±0.4
L	10	0.6 ±0.3	0.8 ±0.1	18	2.6 ±0.5	0.7 ±0.4	10	4.7 ±0.4	0.1 ±0.6
M	16	0.7 ±0.3	0.5 ±0.1	--	--------	--------	--	--------	--------
N	--	--------	--------	9	2.6 ±0.1	0.2 ±0.1	--	--------	--------

of the domination of x. As a result, error estimates are rather large for these cases. However, it is clear that in air the y parameter decreases near the Bragg peak, whereas in nitrogen it has a maximum before it becomes negligibly small.

The survival curves change abruptly beyond the stopping points of primary beam particles, that is, beyond the Bragg peak at positions H to N. Survival curves are nearly exponential at the Bragg peak, but shoulders reappear for curves in the region downstream from the peak. Cell killing here is due to the dose from fragments only.

Confidence Limits for Inactivation Coefficients

When a least-squares fit of the data is made using the logarithm of survival as a weighting function, the Chi-square function near the minimum behaves as a paraboloid. At a given value of Chi-square, determined by the desired probability confidence limit, the values x and y arrange themselves on an error ellipse. In Figure 7 we show some typical error ellipses for neon beams and various experimental points. The major and minor axes of the ellipses are usually skewed against x and y. The significance of this is that x and y are not fully independent variables, but there is a functional dependence of the value of y on the value of x. The skewedness of the error ellipses is observed for both the LQ and LMT models, and also is apparent in the data of Hall *et al.* (26) and of Todd *et al.* (72). In the case of the RS model (not shown), the axes of the error ellipses are usually nearly parallel to the g and r axes, indicating that the lesions (g) and the repair function (r) may be largely independent. Such results suggest to us that the LQ and LMT models are not optimal, and a better model might be found along the lines of reasoning that led to the RS model.

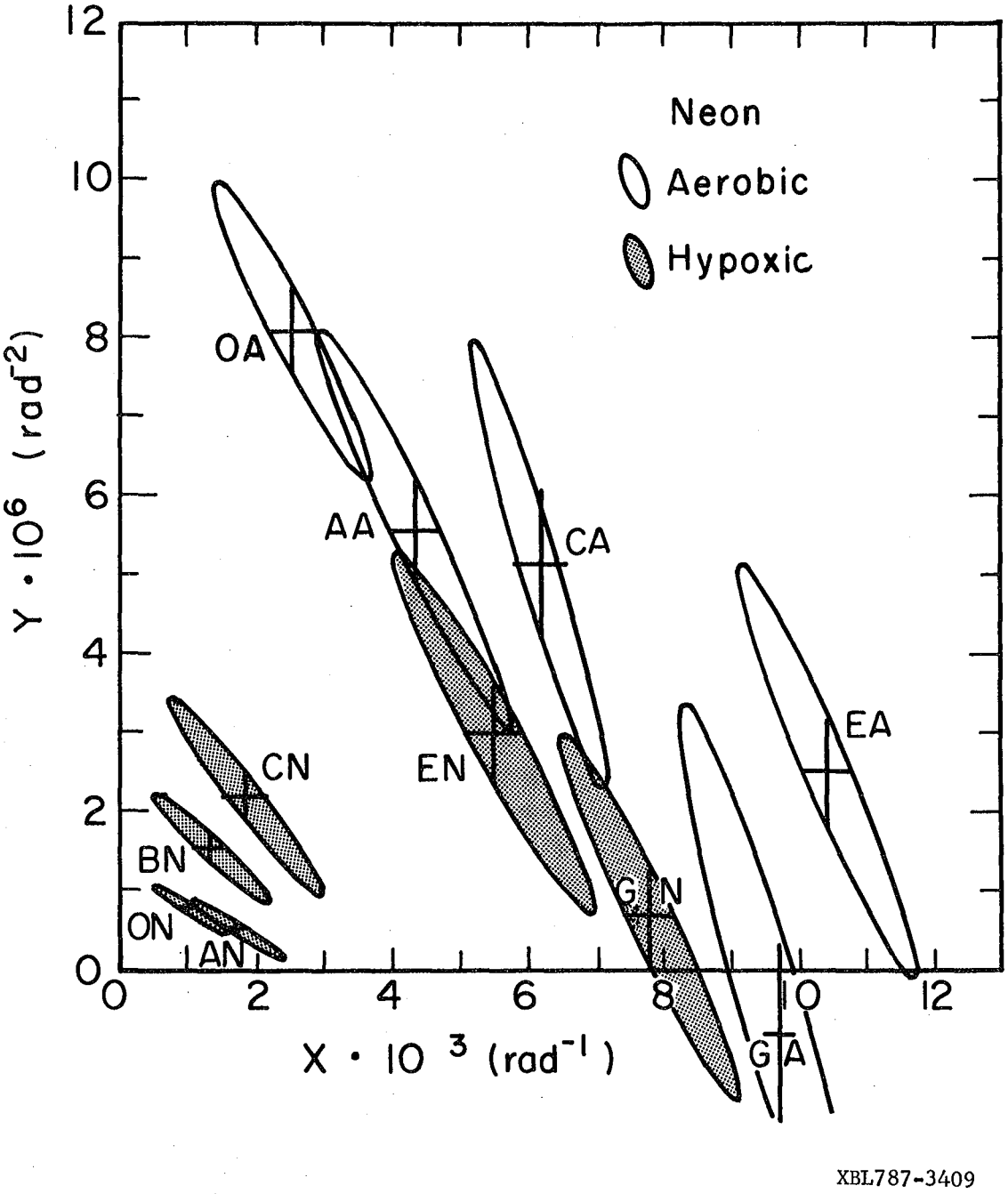

XBL787-3409

Figure 7:

Error ellipses estimated for x and y coefficients for fits of some of the neon data to the linear quadratic model. The letter for each ellipse designates the beam range it represents as depicted in Figure 3.

RBE and OER Values

Figure 8 demonstrates the dependence of RBE on the survival level for neon beams at positions O in the plateau, and C and F near the Bragg peak. There is a clear trend showing that for any of these positions, the RBE increases as the survival probability approaches unity--or as the dose decreases. At the same range and survival level, the RBE for hypoxic cells is greater than the RBE for aerobic cells. For high survival levels (low dose) the RBE is high where the "linear" single-hit killing predominates; for example, in the LQ model for neon position F the hypoxic RBE_{80} = 14.3 ±5.0 and the hypoxic RBE_{10} = 5.3 ±1.3 (see Figure 8).

RBE and OER values at 50% and 10% survival for each of the three beams are given in Tables VA, VB, and VC. Figure 9 demonstrates how the OER and hypoxic RBE at 10% survival varies as a function of residual range for the carbon, neon, and argon beams. Data shown are for the last seven centimeters of track length before the Bragg peak and for four centimeters beyond the peak. For neon and carbon, the RBE_{10} of hypoxic cells is about 1.0 for most of the range, but near the Bragg peak it rapidly increases to values of 5.3 and 4.9, respectively. In contrast, argon beams have a high RBE for most of the range of the particles. Just upstream of the argon Bragg peak, however, a broad maximum peak of 4.4 in the RBE is observed between 1.2 and 0.6-cm residual range; at still lower range values upstream of the peak, the 10% hypoxic RBE decreases to 3.0.

The OER values versus range are also plotted for the 10% survival level in Figure 9. At high velocities both carbon and neon give a value close to that for the control x-rays (2.9). Near the Bragg peak, the OER decreases to low values of between 1.0 and 1.3 for both neon and argon, whereas it is

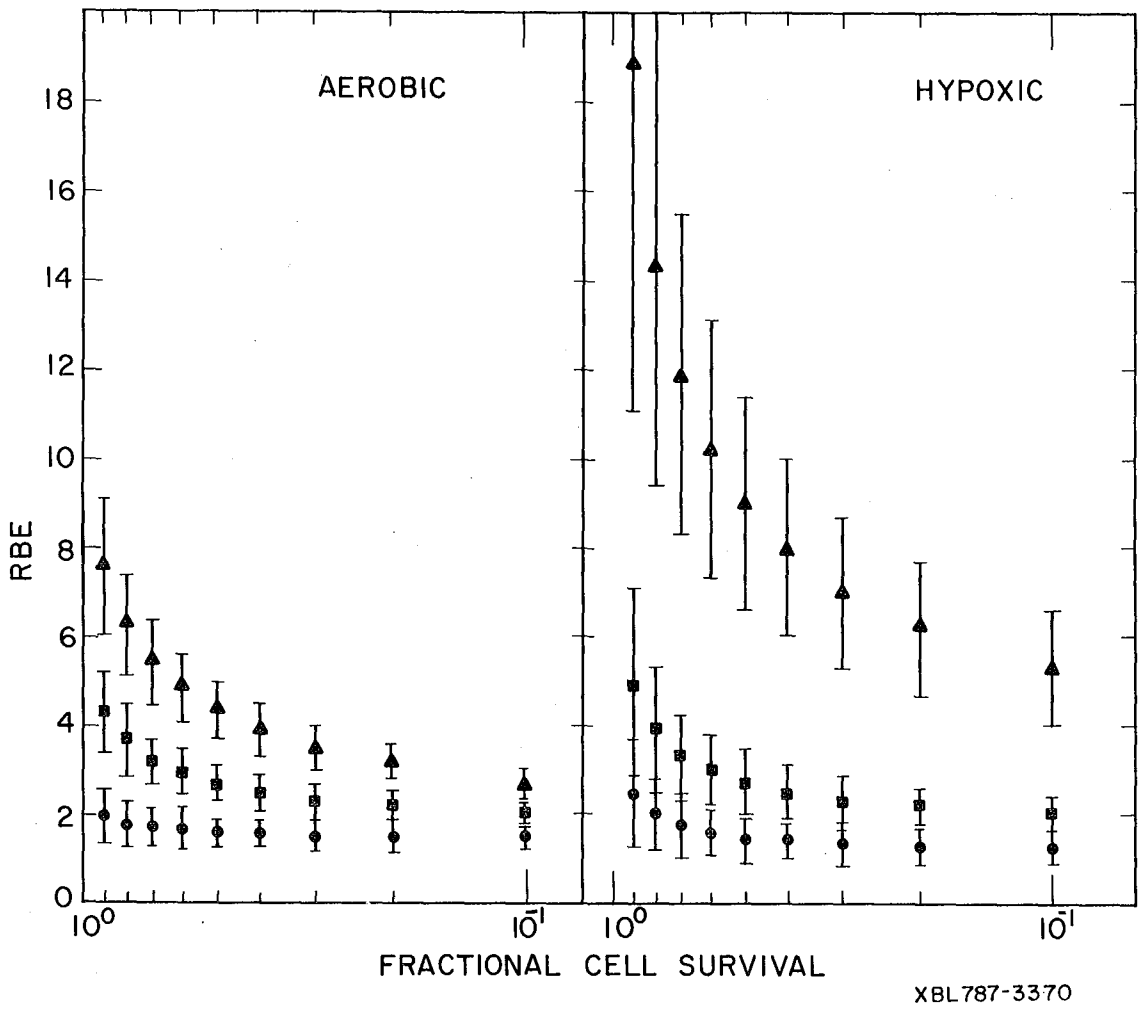

Figure 8:

RBE versus survival level for the neon: position 0 in the plateau (●); position C (■) and position F (▲) near the Bragg peak. Error bars represent 95% confidence limits.

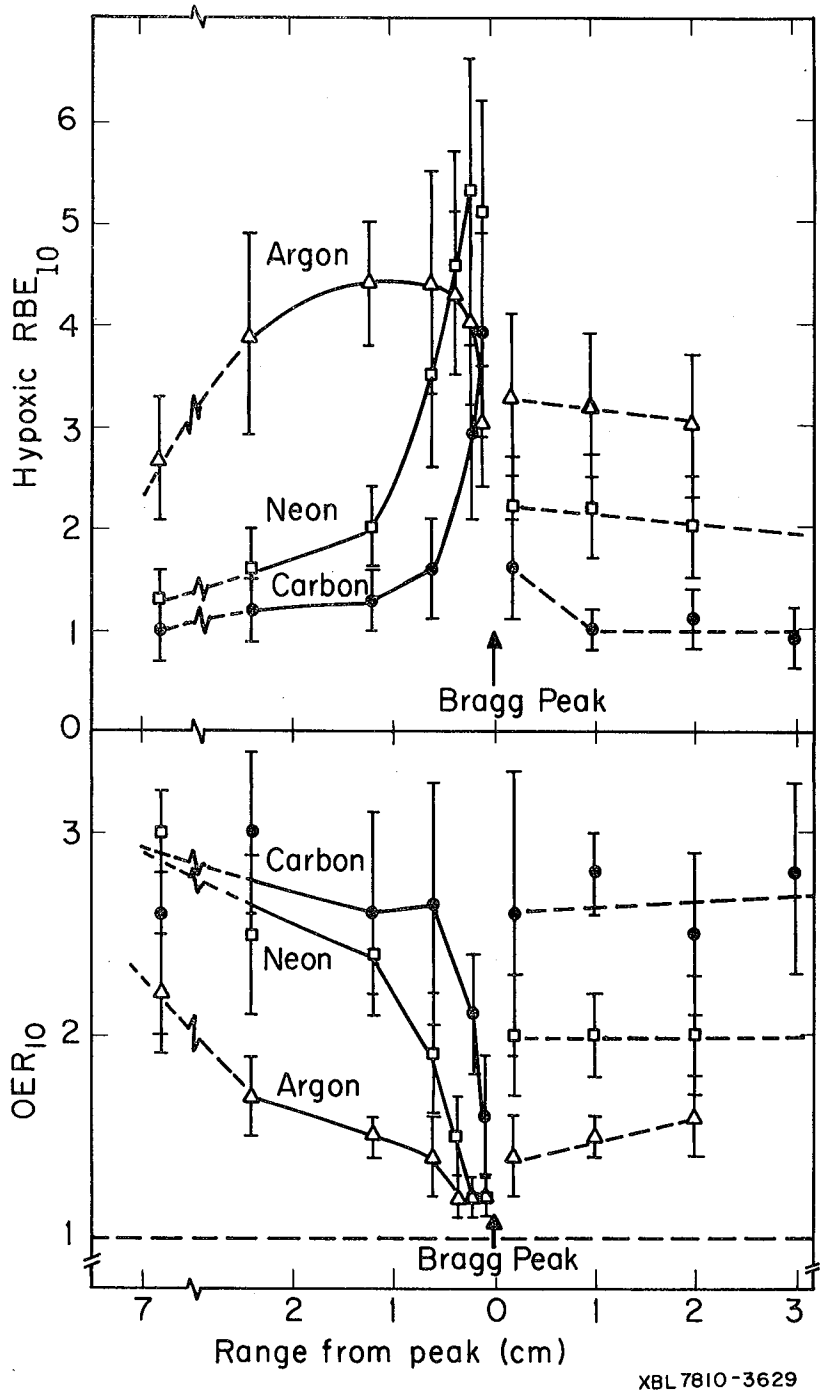

Figure 9:

OER and hypoxic RBE at 10% survival as a function of beam range: carbon (●); neon (■), and argon (▲). Error bars represent 95% confidence interval.

TABLE 5 A. Carbon Beam

POSITION	RBE				OER	
	AEROBIC		HYPOXIC			
	50	10	50	10	50	10
0	1.4 ±0.2	1.1 ±0.2	1.2 ±0.4	0.9 ±0.3	3.0 ±0.5	3.0 ±0.6
0'	1.4 ±0.2	1.2 ±0.2	1.2 ±0.3	0.9 ±0.2	3.1 ±0.3	3.1 ±0.2
A	1.3 ±0.3	1.1 ±0.2	1.3 ±0.5	1.0 ±0.3	2.7 ±0.8	2.6 ±0.6
B	1.9 ±0.3	1.4 ±0.2	1.4 ±0.4	1.2 ±0.3	3.3 ±0.5	3.0 ±0.4
C	1.8 ±0.4	1.5 ±0.2	1.5 ±0.5	1.3 ±0.3	3.1 ±0.7	2.6 ±0.5
D	2.2 ±0.5	1.8 ±0.3	1.8 ±0.7	1.6 ±0.5	3.1 ±0.9	2.7 ±0.6
F	3.7 ±0.6	2.6 ±0.3	3.6 ±1.1	2.9 ±0.8	2.6 ±0.4	2.1 ±0.3
G	3.6 ±0.7	2.6 ±0.4	4.9 ±1.5	3.9 ±1.0	1.9 ±0.4	1.6 ±0.3
H	1.7 ±0.6	1.7 ±0.4	2.3 ±0.7	1.6 ±0.5	1.9 ±0.6	2.6 ±0.7
K	1.3 ±0.2	1.1 ±0.1	1.1 ±0.3	1.0 ±0.2	3.0 ±0.3	2.8 ±0.2
L	1.6 ±0.2	1.1 ±0.1	1.2 ±0.4	1.1 ±0.3	3.3 ±0.6	2.5 ±0.4
M	1.2 ±0.2	1.1 ±0.1	1.1 ±0.4	0.9 ±0.3	2.8 ±0.6	2.8 ±0.5

TABLE 5B. Neon Beam

POSITION	RBE				OER	
	AEROBIC		HYPOXIC			
	50	10	50	10	50	10
O	1.6 ±0.3	1.5 ±0.2	1.5 ±0.5	1.3 ±0.3	2.7 ±0.6	2.9 ±0.5
A	1.9 ±0.3	1.6 ±0.2	1.6 ±0.4	1.3 ±0.3	3.1 ±0.3	3.0 ±0.2
B	2.0 ±0.3	1.7 ±0.2	2.2 ±0.7	1.6 ±0.4	2.3 ±0.4	2.5 ±0.4
C	2.7 ±0.4	2.0 ±0.2	2.7 ±0.7	2.0 ±0.4	2.6 ±0.2	2.4 ±0.2
D	4.2 ±0.7	2.8 ±0.4	5.8 ±1.7	3.5 ±0.9	1.9 ±0.3	1.9 ±0.3
E	4.5 ±0.6	2.9 ±0.3	7.7 ±2.1	4.6 ±1.1	1.5 ±0.2	1.5 ±0.2
F	4.4 ±0.6	2.7 ±0.3	9.0 ±2.4	5.3 ±1.3	1.2 ±0.1	1.2 ±0.2
G	4.3 ±0.6	2.6 ±0.3	8.6 ±2.2	5.1 ±1.1	1.3 ±0.1	1.2 ±0.1
H	2.2 ±0.4	1.8 ±0.3	3.0 ±0.8	2.2 ±0.5	1.8 ±0.2	2.0 ±0.3
K	2.6 ±0.3	1.8 ±0.2	3.2 ±0.8	2.2 ±0.5	2.1 ±0.2	2.0 ±0.2
L	2.4 ±0.4	1.7 ±0.3	3.1 ±0.9	2.0 ±0.5	2.0 ±0.3	2.0 ±0.3
N	1.9 ±0.2	1.4 ±0.1	2.9 ±0.7	1.8 ±0.3	1.7 ±0.1	1.9 ±0.1

TABLE 5 C. Argon Beam

POSITION	RBE				OER	
	AEROBIC		HYPOXIC			
	50	10	50	10	50	10
0	2.7 ±0.6	2.1 ±0.4	3.0 ±0.8	2.2 ±0.5	2.3 ±0.4	2.3 ±0.4
A	3.4 ±0.6	2.5 ±0.3	4.2 ±1.1	2.7 ±0.6	2.1 ±0.3	2.2 ±0.3
B	3.7 ±0.5	2.7 ±0.3	5.7 ±1.7	3.9 ±1.0	1.7 ±0.2	1.7 ±0.2
C	3.8 ±0.3	2.6 ±0.2	5.8 ±0.9	4.4 ±0.6	1.7 ±0.1	1.5 ±0.1
D	3.5 ±0.6	2.5 ±0.3	6.3 ±1.8	4.4 ±1.1	1.4 ±0.2	1.4 ±0.2
E	3.4 ±0.5	2.2 ±0.3	6.9 ±1.6	4.3 ±0.8	1.3 ±0.1	1.2 ±0.1
F	3.2 ±0.4	2.0 ±0.2	6.8 ±1.6	4.0 ±0.8	1.2 ±0.1	1.2 ±0.1
G	2.5 ±0.4	1.5 ±0.2	4.9 ±1.2	3.0 ±0.6	1.3 ±0.1	1.2 ±0.1
H	2.3 ±0.4	1.9 ±0.2	4.3 ±1.2	3.3 ±0.8	1.4 ±0.2	1.4 ±0.2
K	2.5 ±0.4	1.9 ±0.2	4.9 ±1.2	3.2 ±0.7	1.3 ±0.1	1.5 ±0.1
L	3.2 ±0.4	2.1 ±0.2	5.1 ±1.3	3.0 ±0.7	1.6 ±0.1	1.6 ±0.2

about 1.6 for carbon. It is significant that the argon OER values are less than 2.0 for the first 5 cm of range, and they are still depressed to a level of 2.3 at the 12-cm residual range. The lowest OER is not observed where the RBE is highest, but it is seen at the very end of the particle range. This is expected since the OER goes as the ratio $RBE_{aerobic}/RBE_{hypoxic}$, and the hypoxic RBE can continue to rise even though the oxic RBE is decreasing. The OER monotonically decreases with increasing LET up to 250 keV/μm where it appears to level off at higher LET.

Confidence Limits for RBE and OER Calculation (Linear Quadratic Model)

Some recent publications use elaborate statistical analyses to evaluate RBE and OER ratios (72,73). According to the usual definition, RBE and OER are each calculated as a ratio of doses at a selected survival level S.

In the LQ model we have used the following approximations, which were derived from equation (2), for the error in x and y. Assume D to be the statistical variation of the dose when S is constant; this comes from D_x (due to variation of x) and D_y (due to variation of y).

$$\delta D = \frac{1}{2}(\delta D_x^2 + \delta D_y^2)^{1/2} , \qquad (6)$$

where

$$\delta D_x = \frac{\delta x \cdot D}{x + 2D \cdot y} , \qquad (7)$$

and

$$\delta D_y = \frac{\delta y \cdot D^2}{x + 2D \cdot y} \quad . \tag{8}$$

Here, D is the dose in air for survival level S. Similar calculations can be used for aerobic and hypoxic data.

This method gives equal weight to errors in x and y. As more accurate data and better models become available, it might be advisable to depart from equal weighting for the parameters of the models. For example, at very high LET, the values of x are determined more accurately than the values of y.

DISCUSSION

Comparison with Other Available Data

Soon after high energy heavy-ion beams became available at Princeton and at Berkeley, there were initial assessments of the effects of 3.9-GeV nitrogen and of 5.4-GeV oxygen particle beams.

Todd grew M3-1F3 hamster cell colony isolates on the walls of tissue culture flasks and exposed these tangentially to monoenergetic beams (74,75), Hall and Lehnert (76) made OER determinations on V79 cells at the nitrogen ion Bragg peak, and found an OER value of 1.25. Another study was made with bean roots (77). Roisman et al. (78), Tobias (79), and Kalofonos (80) also studied survival as a function of residual range with hypoxic and aerated human kidney cells. They used a monoenergetic "submarine" technique, and found that the oxygen effect at the Bragg peak was much lower than at the plateau. In general, the results of earlier studies with mammalian cells agree with this paper. Several proton, helium, and heavy-ion studies with modified beams (having extended Bragg peaks) have been reported in the literature (30-33; 81-85); however, these studies are not easily compared to our data.

Recently Hall et al. (26) measured RBE values for the unmodified 429-MeV/amu argon beam with the V79 cell line using low-density cell suspensions in 2.5-mm diameter sealed plastic ampules. For OER measurements, high density cell cultures were used to metabolically deplete the oxygen supply. These cells were sealed in 4-mm diameter glass ampules. They measured an aerobic RBE_{10} of 2.4 in the plateau, ascending region, and "tail" of the depth-dose curve, and 1.5 at the Bragg peak. These values may be compared to our results of 2.5 at the same plateau range, 2.6 to 2.5 for the ascending region, 1.5

at the Bragg peak, and 1.9 in the tail. OER values at 10% survival were 2.0 in the plateau, 1.45 in the ascending region, 1.32 in the peak, and 1.5 in the tail. These can be compared to our OER values of 2.2, 1.5 to 1.4, 1.2, and 1.5 for the respective comparable ranges. Therefore, despite major differences in technique and working with different cell lines, the RBE and OER values reported for argon were not significantly different in the two sets of experiments.

The inactivation coefficients for the linear quadratic model which we report generally do not agree with those of Hall et al. (26). They showed that the best fit aerobic linear coefficient decreased with increasing LET from the plateau to the peak of the 429 MeV/amu argon beam. In contrast, our results show that for the human kidney cell the aerobic and hypoxic linear coefficient increases with increasing LET (up to about 200 to 300 keV/μm), and then levels off over several centimeters upstream of the peak of the 570-MeV/amu argon beam before it begins to decrease. They also reported that the quadratic coefficient increased with increasing LET (although their best fits had sizeable error estimates). In contrast, we see a definite decrease in the aerobic best fit y coefficient with increasing LET. The best fit hypoxic y coefficients are uniformly low over the LET range studied, except for an increase noted in the range of 80 to 200 keV/μm.

LET Dependence of Survival Parameters

The results reported in this paper have demonstrated the dependence of survival parameters on the residual range of particle beams. Further insight might be gained by considering LET, particle charge, and particle velocity.

For the LQ model, the variation of the inactivation coefficients x and y, as functions of mean LET is shown for aerobic exposures in Figure 10 and for hypoxic exposures in Figure 11. The dependence of RBE on LET is shown in Figure 12.

As already noted by Chapman et al. (86) and Cox (9) for V79 cells, the x values for both aerobic and hypoxic cells increase rapidly with increasing LET. However, Chapman used the extended Bragg peaks to irradiate cells in suspension, which represents a broader mixture of LET than has been used in this report, and he therefore could not get many survival measurements above 100 keV/μm with these beams.

Inspection of Figures 10, 11, and 12 shows that mean LET_∞ can be used to characterize RBE and the linear inactivation coefficients for all three beams. Each set of data lie on a single curve up to about 100 keV/μm when plotted as a function of mean LET_∞. This appears to be true for both aerobic and hypoxic conditions. The 95% confidence limits are too large to tell whether or not the data for each particle should be represented by a separate curve. Above 100 keV/μm mean LET_∞ does not uniquely characterize either RBE or x; the curve separates, and x and RBE values are lower for argon and higher for neon ions. It is also interesting to note that the maximum values for the x coefficient in an aerobic environment are observed at a lower LET (140 keV/μm in Figure 10) than can be seen under hypoxic conditions (200 keV/μm in Figure 11).

The separation of the x and RBE curves beyond 100 keV/μm in these cell killing effects might be caused either by the velocity dependence of these

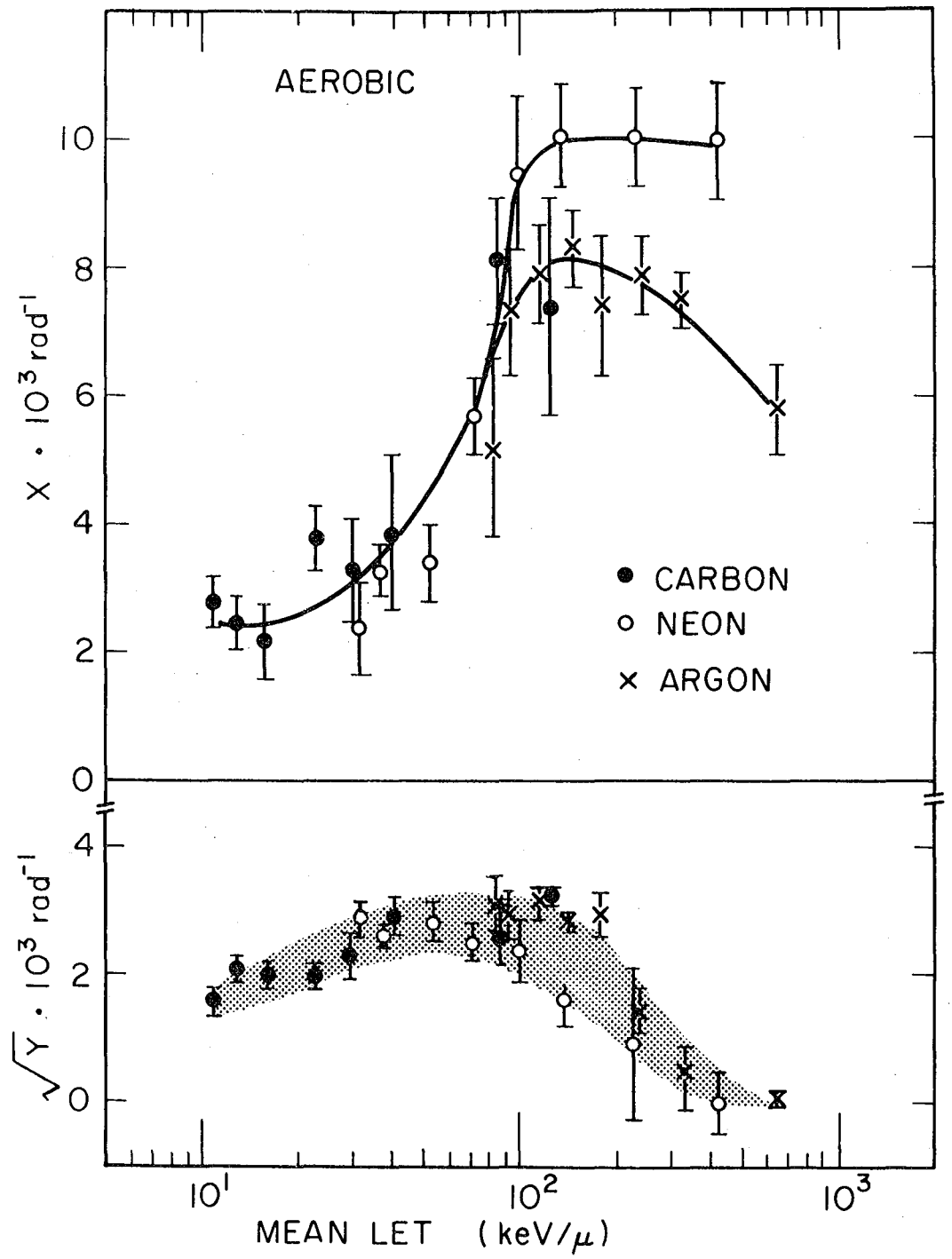

Figure 10:

Linear quadratic coefficients x and $\sqrt{y}$ as a function of dose-average mean LET for aerobic survival. Error bars represent 95% confidence interval.

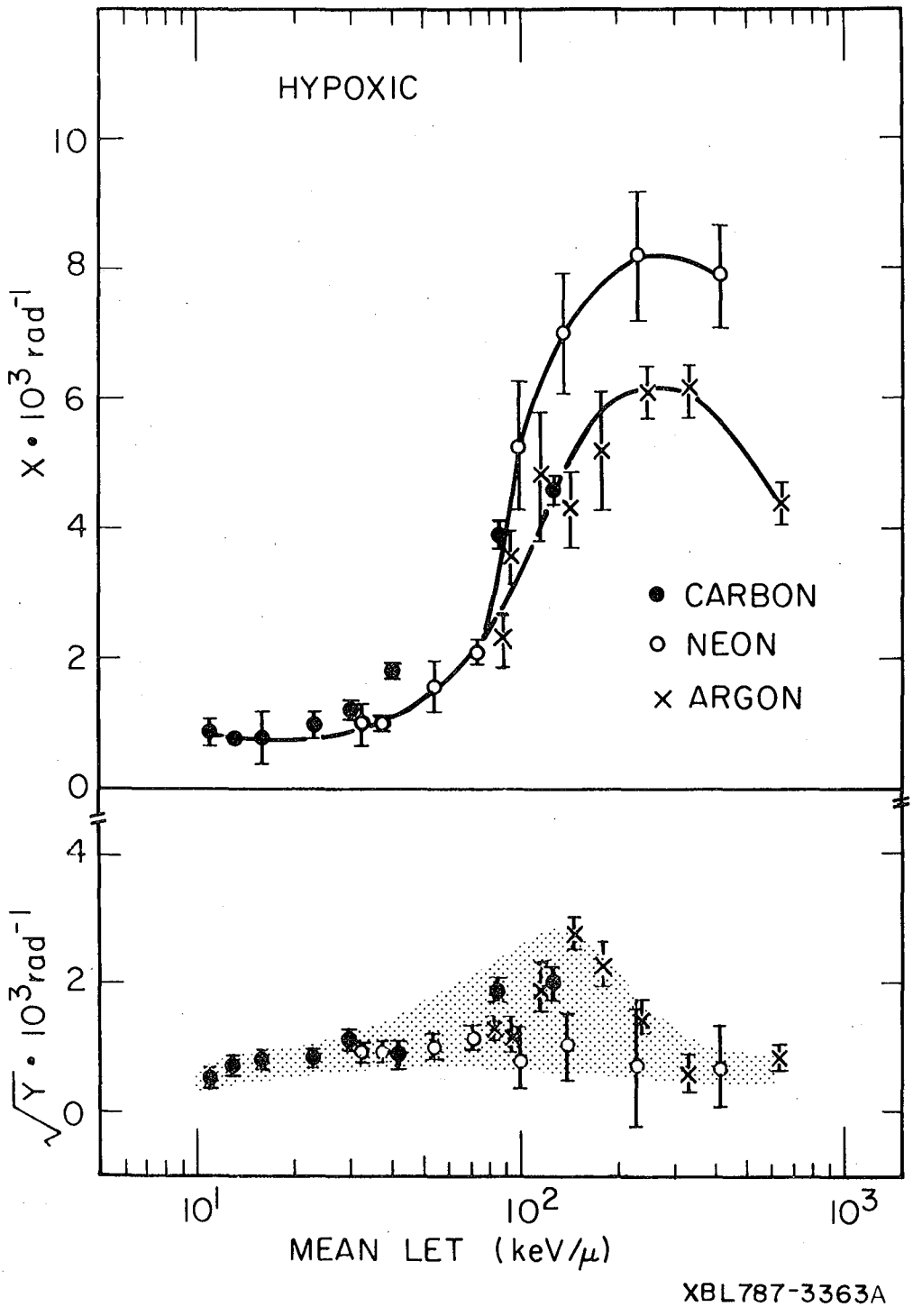

Figure 11:

Linear quadratic coefficients x and $\sqrt{y}$ as a function of dose-average mean LET for hypoxic cell survival. Error bars represent 95% confidence interval.

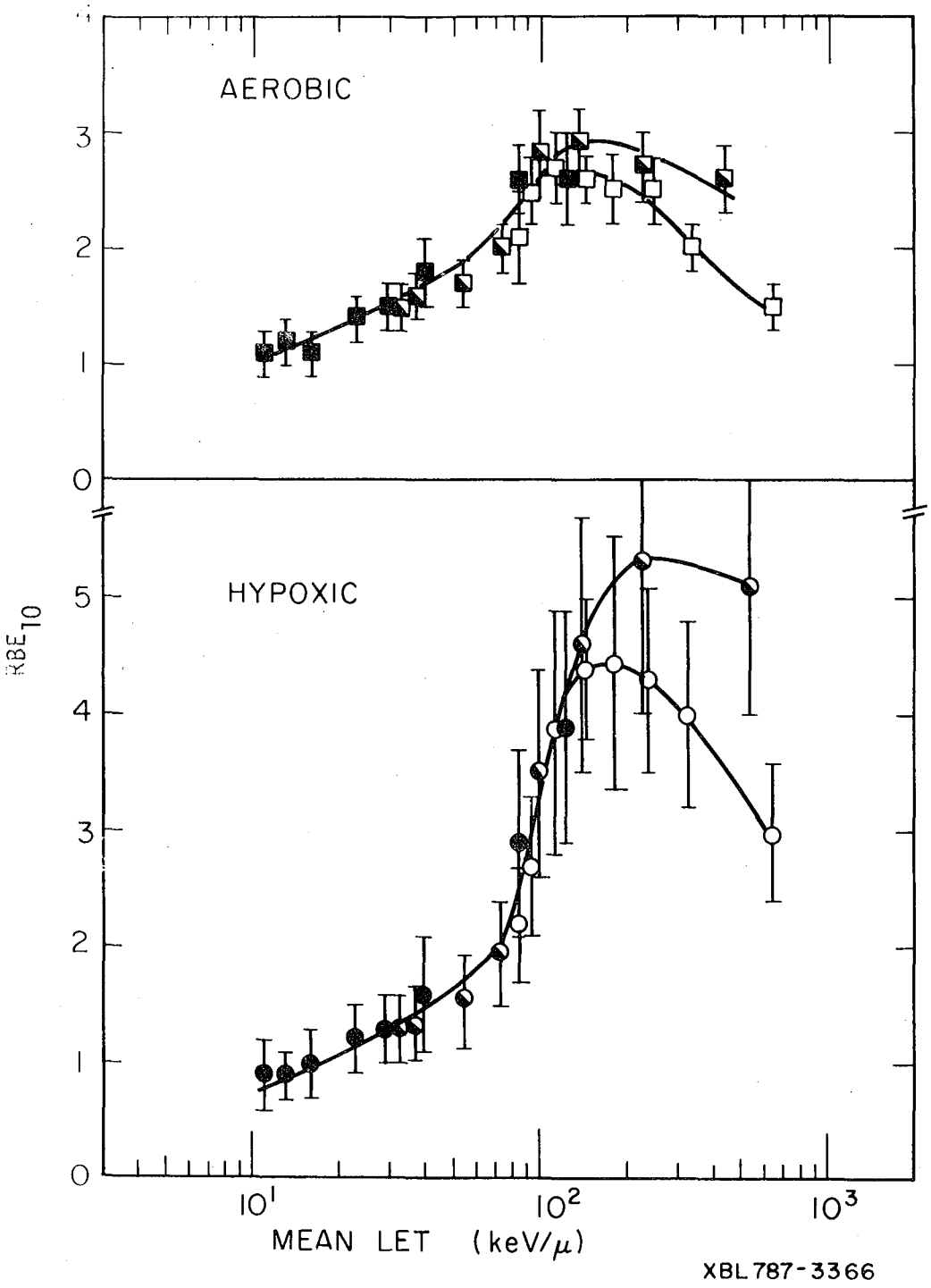

Figure 12:

RBE at 10% survival as a function of the dose-average mean LET: carbon data (●, ■), neon data (◔, ◪), and argon data (○, □). Error bars are for 95% confidence limits.

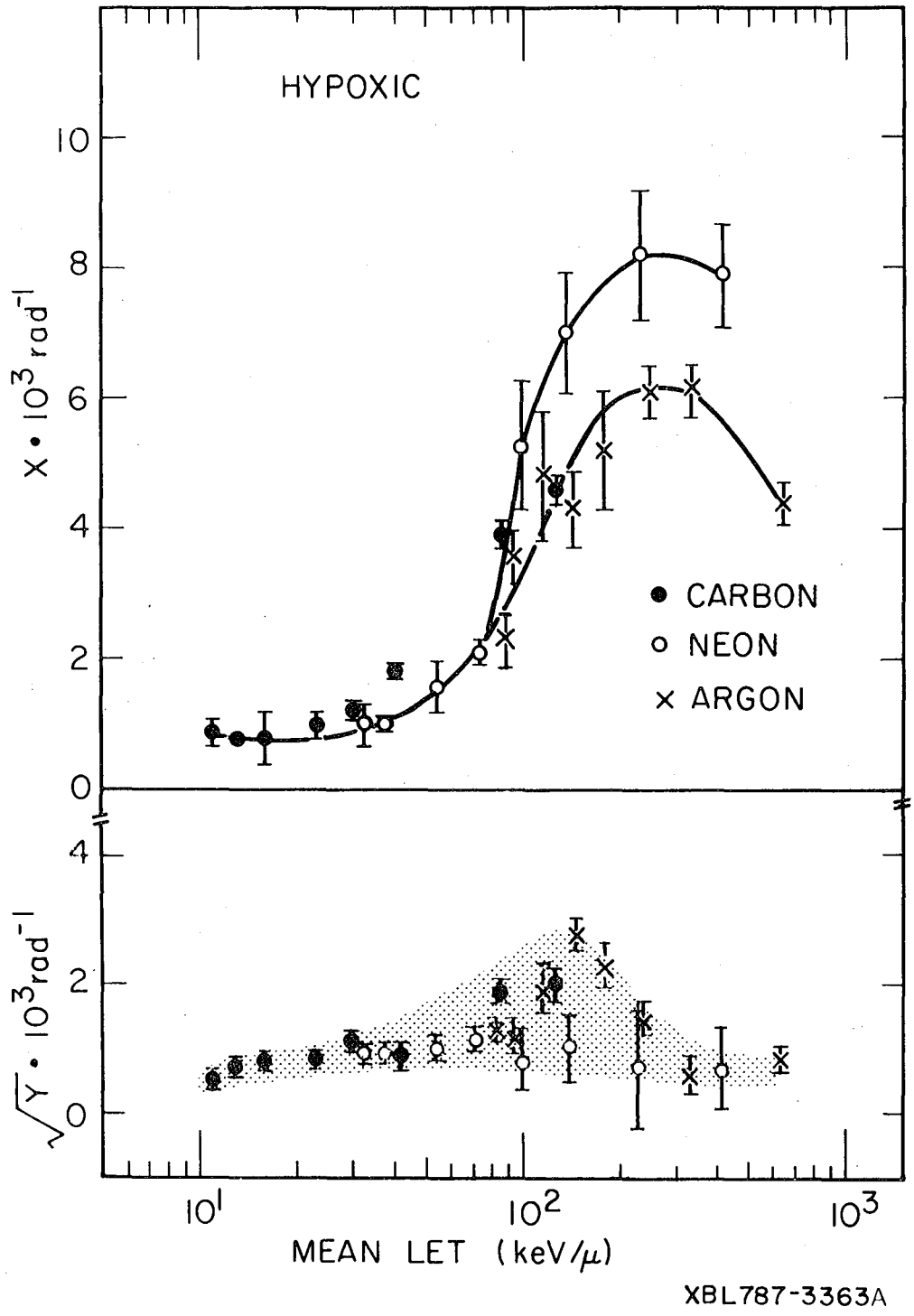

Figure 11:

Linear quadratic coefficients x and $\sqrt{y}$ as a function of dose-average mean LET for hypoxic cell survival. Error bars represent 95% confidence interval.

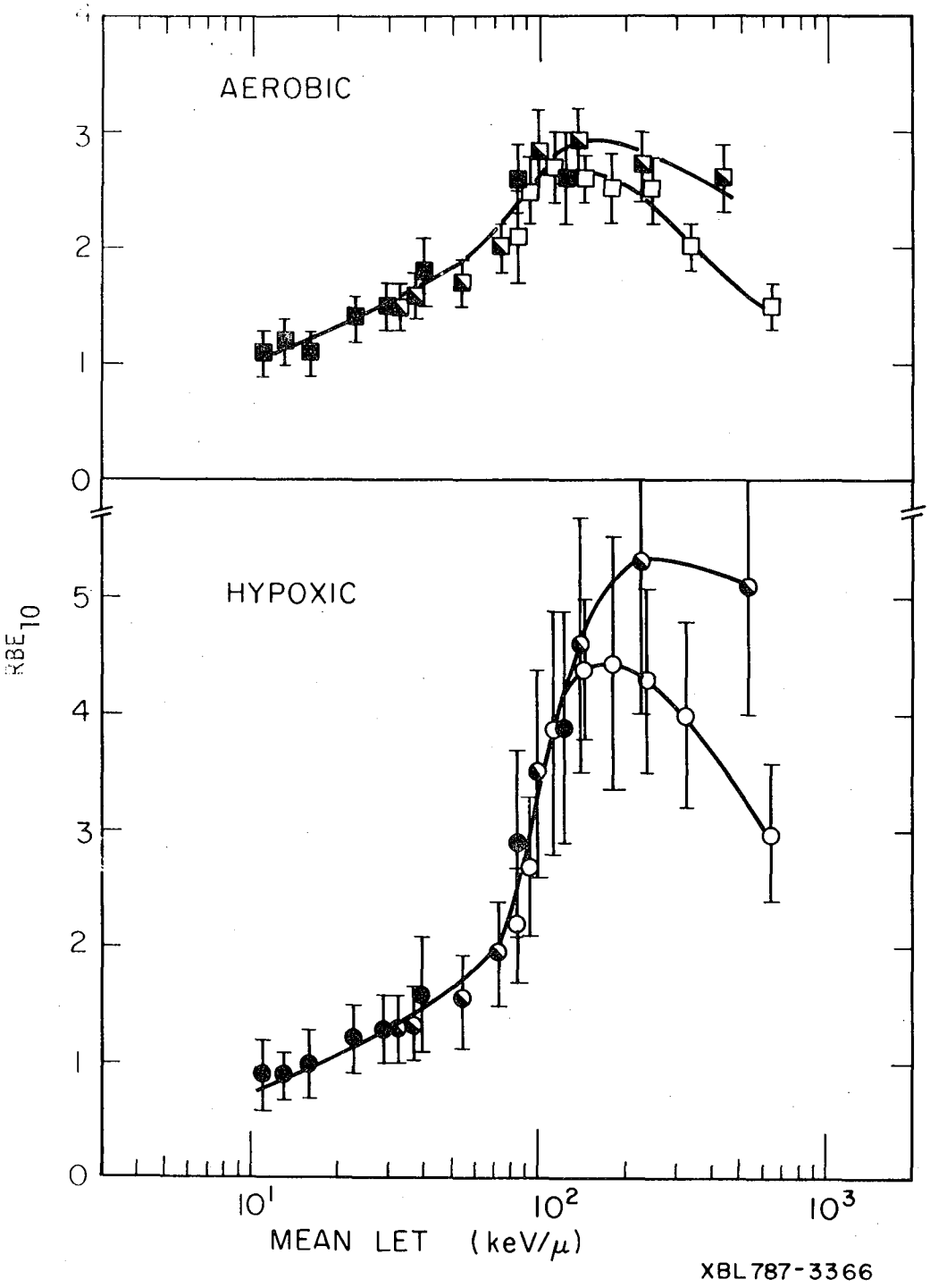

Figure 12:

RBE at 10% survival as a function of the dose-average mean LET: carbon data (●,■), neon data (◐,◪), and argon data (○,□). Error bars are for 95% confidence limits.

effects or by the presence of different amounts of fragmentation--or both. We know that the argon beam fragments much more than neon (see Table IB and IC), and we think that the fragmentation process can account for most of the difference. We have, however, attempted to estimate the magnitude of effects due to fragments in order to arrive at a description of the particle effects due to the primary beam alone.

Rossi (87) has theorized that the quadratic coefficient $\underline{y}$ is constant and independent of LET. In contrast, the plots for $\sqrt{\underline{y}}$ in Figures 10 and 11 show that $\underline{y}$ is not independent of LET. For aerobic conditions, $\sqrt{\underline{y}}$ has a broad maximum below 100 keV/μm; under hypoxic conditions $\sqrt{\underline{y}}$ has low values at low LET and a broad maximum is reached at about 150 keV/μm. At still higher values of LET the $\sqrt{\underline{y}}$ values for hypoxic and oxic conditions overlap and $\sqrt{\underline{y}}$ decreases to such low levels that the survival curves are nearly exponential at very high LETs. There is also some suggestion in Figures 10 and 11 that the values of $\sqrt{\underline{y}}$ for argon lie above those for neon; however, we cannot prove this with statistical significance. In an analysis of chromosome effects, Neary did postulate a disappearance of $\underline{y}$ at high LET (63).

It is well known that heavy ions have good depth-dose distributions (79), and one of the major results of this paper is to show that the RBE for heavy particles is high near the Bragg peak while it remains lower at the plateau. These differences are accentuated at low dose. The practical consequence of these observations is that when a heavy-ion beam actually strikes a tissue target, the depth survival effect depends both on the dose and the RBE at each depth. These two factors reinforce each other, and therefore the lethal effect in the region of the Bragg peak of each of the three particle beams as reported here is significantly greater than at the plateau.

LET Dependence of OER

In the Bragg peak region of the carbon, neon, and argon beams, OER values were significantly reduced relative to 220-kVp x rays. OER values approaching 1.0 were generally observed. Most notable is the fact that in general, heavier ions have lower OER values for a larger portion of their range than do lighter ions. In addition, we note that the lowest OER is not always observed where the RBE is highest (see argon results). Instead, the OER appears to decrease continuously with increasing LET, especially at LET values near 100 keV/μm, before leveling off near 250 keV/μm. Presumably, the very lowest OER occurs where the transferred energy density along the particle tracks in the hypoxic cells is high enough to produce a lethal effect even without help from oxygen molecules.

Since fragment particles have generally lower atomic numbers, and, in the case of glancing collisions, higher velocity than the primary beam particles, the OER of the fragments is higher than that of the primary particles. In fact, the OER of the fragments that appear just beyond the Bragg peak decrease with increasing atomic number of the primary beam. Upstream of the Bragg peak the OER of the whole beam (fragments and primary particles) is therefore somewhere in between the OER of the pure primary particles and fragments present at each residual range.

Unlike the RBE values, the OER values do not appear to have remarkable changes with survival level. It appears that both linear and quadratic components of the survival curve have an oxygen effect about equal in magnitude at low LET. At high LET, the OER of the linear component becomes nearly one. We suspect that the quadratic component still has a significant OER; however,

we cannot state this with certainty because of the dominance of the linear survival component at high LET.

The dependence of OER on mean LET_∞ is shown in Figure 13, where all experimental points for carbon, neon, and argon are plotted. Figure 13 also has OER data from Barendsen (23) using low-energy helium ions and low-energy heavy ion data from various ion species from Todd as analyzed by Bewley (88). Interestingly, the trend of our data follows that of Barendsen's remarkably well, except that Barendsen's OERs are lower for all LET points and also for x rays.

Todd's data, however, show a reduced OER at a much lower LET. We believe that the discrepancy between the three curves may be due in part to the presence of low-LET fragments in the Bevalac beams. Despite the separation of the curves at low LETs, all three studies agree that the OER becomes 1.2 or less at greater than about 200 keV/μm.

Velocity and Charge Dependence of Lethal Effects

From Figures 10 through 13 it is evident that dose average LET is not an adequate variable to describe the effects of heavy particles and their fragments. An additional variable, such as the charge of the particle, seems essential.

In a theoretical paper in 1965, Turner and Hollister (89) demonstrated that, with certain assumptions, particle charge and velocity are independent variables with respect to RBE. They suggested that relative effectiveness is a function of Z^2 and of particle velocity. Katz further advocated the use of the quantity $Z\beta^{-\alpha}$, where α depends on the range energy relationship (90). An analysis by Bewley (88) of the LET dependence of the oxygen effect

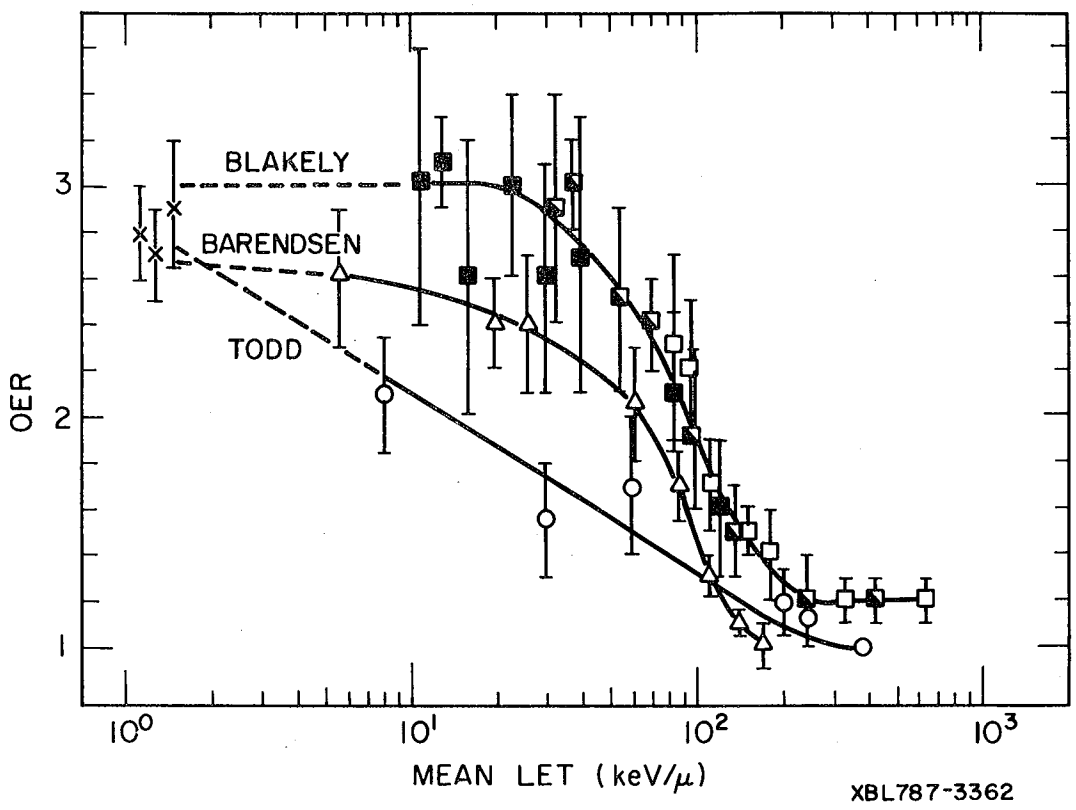

Figure 13:

OER (95% confidence limits) versus dose-average mean LET: carbon (■), neon (▣), and argon (□) beams from the Bevalac by Blakely et al.; Barendsen (△) low-energy helium ion data (15), Todd (○) high-energy (up to 10 MeV/amu) heavy-ion data (3), and x-ray data (X).

demonstrated some apparent inconsistencies between the low-energy heavy-ion and helium data. Curtis (91) and later Katz et al. (92), proposed that the ratio of charge to velocity was a more important parameter than LET.

More recently Chatterjee and Tobias (93) suggested that not LET, but perhaps the radial distribution of energy density in the core and penumbra of the heavy particles is important. In their model it is assumed that the radiobiological action depends on cooperative interactions between diffusing free radicals in the particle track.

In order to test the dependence of biological effects on particle velocity, we restricted ourselves to an analysis of the linear coefficient x of the LQ model. It was necessary to estimate the x contributions of the primary beam particles and of the fragments, which were assumed to be in linear relationship with each other. For a given dose D:

$$xD = (x_p D_p) + (x_f D_f), \tag{9}$$

where the subscript p stands for primary particles and f stands for fragments. There are probably interactions between the primary beam and fragments that can cause biological effects. However, we ignore this possibility in equation (9) because our analysis is a first approximation only; when more accurate data are obtained, it may be necessary to refine the analysis.

First, for each experimental point we used the dose fraction from fragments as seen in column V of Table I, and dose-average LET values for primary particles (column VIII), and for fragments (column IX) in the beam. Next, we estimated x_f for the fragment beam. This could be done approximately on

the basis of available data. Values for the linear inactivation coefficient x_p for primary fragments were then calculated on the basis of equation (9).

Next, we have plotted cell inactivation cross sections σ_{xp} for the primary particles as a function of $1/\beta^2$ (see Figure 14). The values of σ_p are based on the relationship:

$$\sigma_{xp} = \phi x_p \cdot L_p \,, \tag{10}$$

where L_p is the LET_∞ of the primary beam and ϕ is a constant dependent on the units of x_p and L_p.

The results are shown in Figure 14. The solid lines represent a theoretical expression for the cross section σ:

$$\sigma = \sigma_{min} + \sigma_{max} \left[1 - \exp\left(-aZ^h/\beta^k\right)\right] \,, \tag{11}$$

where σ_{max} represents the saturation value of the cross section and $\underline{a}$ is a constant that depends on the gas milieu; σ_{min} represents a limiting cross section for values of β near unity at very high kinetic energies where the track structure is lost, and the radiation effects resemble those from low-LET radiation. The exponent $\underline{k}$ relates to the effect of velocity on the radial structure of energy transfer, and should be independent of the atomic number. The exponent $\underline{h}$ relates to the charge dependence of energy transfer and should be independent of the velocity. From previous work (60) we know that $\underline{h}$ should be about 4. Table VI represents the values for the solid-line curves in Figure 14.

A separate curve is obtained for each particle beam (carbon, neon, and argon). We find, as expected, that the three curves are spaced by the approximate factor of the ratio of Z^4 values. For hypoxic cells the data agree with a slope of $Z^4/\beta^{4.6}$, and for aerated cells the slope is Z^4/β^4.

The aerobic slopes of Z^4/β^4 agree with the general representation suggested by Curtis.[8] However, the description of saturation effects at low β values cannot be accurately inferred from the data in this paper. The hypoxic curves represent a degree of decoupling between Z and β, since these appear with different exponents (4 and 4.6, respectively). This is to be expected, since Z^2 relates to the total energy transferred, whereas β also determines the radial energy distribution.

Equation (11) was derived on the assumption that for the linear component of survival curves, the lethal events are proportional to the square of the local energy deposition in the track. We expect that equation (11) would hold more accurately in the middle energy domain than at very low or very high energies. At low energies there is a mixture of velocities because of straggling. At high energies, the effect due to straggling becomes negligible. When monoenergetic beams are available at several discrete energies without fragments, it will be possible to study the functional relationships more accurately.

The results above indicate that the description of the biological effects of heavy ions require at least three variables. Convenient variables may be fluence, particle velocity, and charge. Alternatively, the effects can be described in terms of dose, mean LET_∞, and charge.

If the variation of the σ_x coefficient obtained under hypoxia depended only on LET_∞, then we would expect that the slope would be some power of

TABLE VI. Cell Inactivation Coefficients for Equation (11)

	σ_{min} (micron^2)	σ_{max} (micron^2)	a	h	k
Exposure in air	0.3	140	2.3×10^{-3}	4	4
Exposure in nitrogen	0.1	130	5.4×10^{-4}	4	4.6

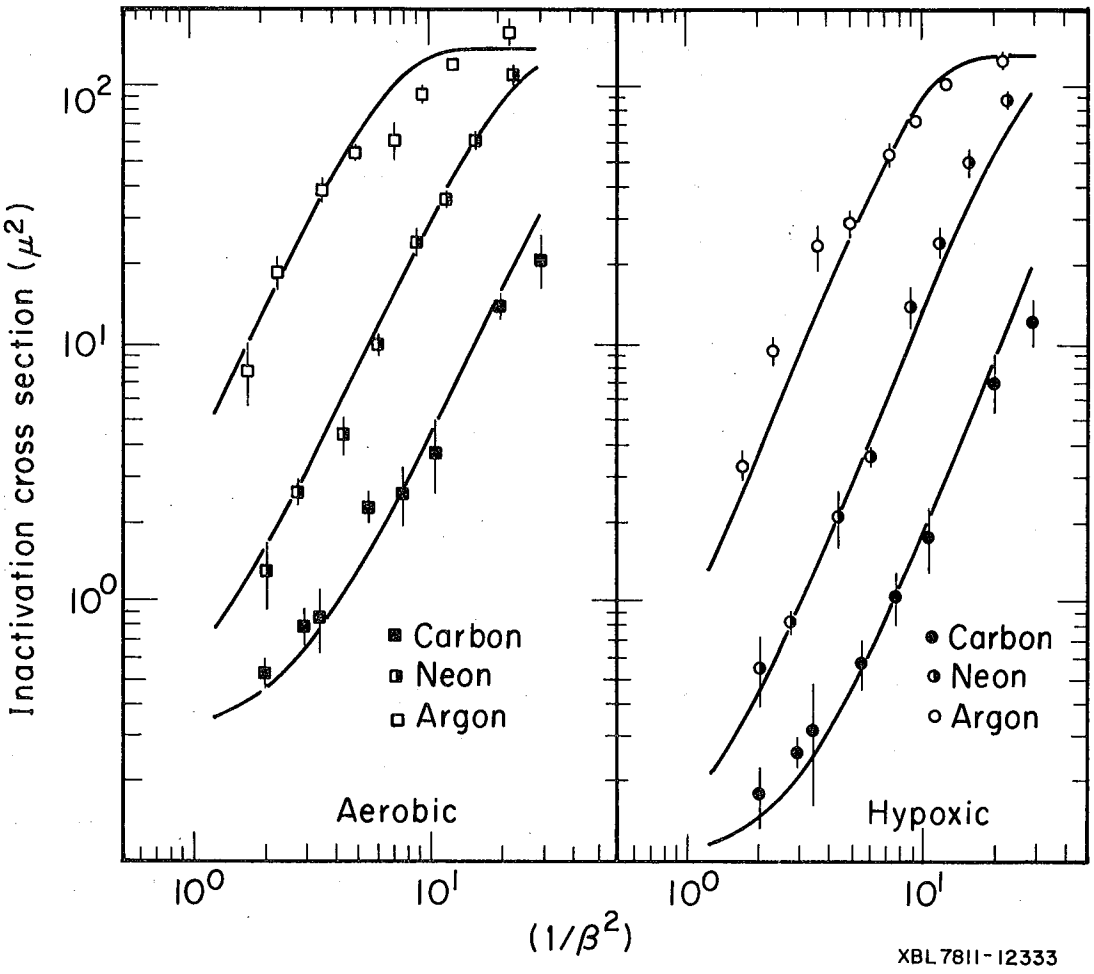

Figure 14:

Cell inactivation cross-section versus $1/\beta^2$.

Z^2/β^2, because LET is proportional to Z^2/β^2 (except for a slowly varying logarithmic term). The relationship we obtained can be expressed instead as proportional to $\beta^{-0.6} \times (L_p)^2$. The term $\beta^{-0.6}$ indicates a velocity dependence of σ_x. We know from Bethe's theory that the radial structure of the ionizing track is dependent on β, but is independent of the atomic number. Therefore, we may assume that the $\beta^{-0.6}$ term is an expression of the effect of the radial structure of the track. The cross sectional area of the track core increases slowly with β and the density of the tranferred energy becomes correspondingly smaller (94). We know, however, that diffusion-controlled free-radical chemistry is also an important factor (95).

When the cell inactivation cross section for hypoxic cells is plotted as a function of LET_∞, a separate curve describes the effects of each particle. Using the relationships obtained with the analysis above, we plotted the L dependence in Figures 11 and 12.

We used the LQ survival hypothesis to test the velocity dependence of the linear term. In the LQ and the LMT models, the linear term indicates the lethal effect caused by a single particle crossing the nucleus. There is no explicity linear term in the RS model, however, the model still fits the data because the value for σ_{xp} can be derived from equations (4) and (10):

$$\sigma_{xp} = \frac{g}{r+1} \cdot L_p \quad . \tag{12}$$

In terms of the RS model, then, the rise of σ_{xp} with L_p can also be interpreted as due in part to a decrease in repair probability measured by r.

We are not convinced that any of the above models can adequately describe all the observed phenomena. In the "repair-misrepair" model recently developed (96), σ_{xp} describes the competition between "perfect" repair and "misrepair," and it is also dependent on the conditions for repair.

The velocity and charge dependence of these effects are fundamental to our understanding of the biological response to charged particles. This information may enable us to model biological effects in combined high and low LET distributions from beams that have been range filtered for therapeutic purposes.

In addition, insofar as the kidney cells may be good models for human tumor systems, the data may be useful to predict the biological response to beams of intermediate atomic number. For example, it appears that for optimal reduction of the oxygen effect for certain tumors, perhaps a particle beam heavier than neon should be used. It is also likely that a beam between neon and argon in atomic weight (e.g., silicon 28 or phosphorous 31) would still have an OER advantage, and would generally produce less fragmentation and less overkill effect than an argon beam.

CONCLUSION

We have obtained a set of consistent data on the lethal cellular effects of carbon, neon, and argon particles as a function of a broad range of particle velocities. In general, the effects followed previous predictions with respect to increased and saturating biological effectiveness as the velocity was decreased and the particle charge increased. The lowest oxygen effects were noted for argon over a considerable spread of velocities.

We have evidence that mean LET_{∞} is not a completely adequate variable for predicting biological effects. Though the data show considerable scatter a method was developed for quantitating biological effect as a function of particle charge and velocity--two separate variables. More accurate data are important for further development of these concepts.

ACKNOWLEDGEMENT

The authors would like to acknowledge the excellent technical assistance of I. Madfes, L. Craise, and J. Howard. We have also appreciated the help of J. D. Chapman, A. Beckmann, D. Kalofonos, B. Martins, R. Roisman, R. Roots, M. Yezzi, F. Abrams, C. Perez, P. Chang and the outstanding cooperation of E. Lofgren, H. Grunder, F. Lothrop, R. Force, M. Tekawa, and the Bevalac crew, including T. Criswell, K. Crebbin, G. Welch, S. Nissen-Meyer, E. Schneider, R. M. Larimer, D. Love, L. Kanstein, and F. Yeater. We wish to thank A. Chatterjee, J. Magee, F. Ngo, S. Curtis, T. Tenforde, and E. Alpen for their helpful discussions. We thank R. Stevens for assistance in drafting figures, and M. C. Pirruccello for her editorial assistance.

This investigation was supported by the Biomedical and Environmental Research Division of the Department of Energy, and by the National Cancer Institute Grant CA-15184.

NOTES

1. Kindly provided by G. W. Barendsen of the TNO Radiobiology Laboratories, Rijswijk, Netherlands.

2. Designed by one of us (CT) and constructed in the Donner Laboratory Shop under the direction of Edward F. Dowling.

3. We are indebted to J. Howard and the Bevalac crew for their outstanding assistance.

4. Developed by J. R. Alonso and J. Howard.

5. Courtesy of T. S. Tenforde.

6. Done with the assistance of R. H. Thomas and T. M. de Castro of LBL's Environmental Health and Safety Department.

7. We are grateful for consultations with Dr. Norman Albright of LBL with regard to statistical methods.

8. S. Curtis used the notation Z^{*2}. In our paper Z means the actual charge; for most of the range this is equal to the atomic number of the particle.

REFERENCES

1. H. CHAMBERS and S. RUSS, The action of radium radiations upon some of the main constituents of normal blood. Proc. Roy. Soc. London B 84, 124-136 (1912).

2. R. E. ZIRKLE, Biological effects of alpha particles. In Biological Effects of Radiation (B. M. Duggar, Ed.). McGraw Hill, New York, 1936.

3. P. W. TODD, Reversible and irreversible effects of ionizing radiations on the reproductive integrity of mammalian cells cultured in vitro. PhD Thesis, University of California, Berkeley, 1964.

   P. W. TODD, Heavy-ion irradiation of cultured human cells. Radiat. Res. Suppl. 7, 196-207 (1967).

4. G. W. BARENDSEN, Responses of cultured cells, tumors and normal tissues to radiations of different linear energy transfer. In Current Topics in Radiation Research (M. Ebert and A. Howard, Eds.), vol. IV, pp. 293-356. North Holland Publishing Co., Amsterdam, 1968.

5. L. D. SKARSGARD, B. A. KIHLMAN, L. PARKER, C. M. PUJARA, and S. RICHARDSON, Survival, chromosome abnormalities, and recovery in heavy-ion and x-irradiated mammalian cells. Radiat. Res. Suppl. 7, 208-221 (1967).

6. R. A. DEERING and R. RICE, JR., Heavy-ion irradiation of HeLa cells. Radiat. Res. 17, 774-786 (1962).

7. U. MADHVANATH, M. R. RAJU, and L. S. KELLY, Survival of human lymphocytes after exposure to densely ionizing radiations. Radiation and the Lymphatic System. ERDA Symposium Series 37, 125-139 (1976).

8. R. J. BERRY, Reproductive survival and hypoxic protection as a function of radiation ionization density. Radiat. Res. 70, 355-361 (1977).

9. R. J. COX, J. THACKER, D. T. GOODHEAD, and R. J. MUNSON, Mutation and inactivation of mammalian cells by various ionizing radiations. Nature 267, 425-427 (1977).

10. D. O. SCHNEIDER and G. F. WHITMORE, Comparative effects of neutrons and x rays on mammalian cells. Radiat. Res. 18, 286-306 (1963).

11. F.Q.H. NGO, A. HAN, H. UTSUMI, and M. M. ELKIND, Comparative radiobiology of fast neutrons: Relevance to radiotherapy and basic studies. Int. J. Radiat. Oncol. Biol. Phys. 3, 187-193 (1977).

12. H. SCHLAG, K. F. WEIBEZAHN, and C. LUCKE-HUHLE, Negative pion irradiation of mammalian cells. II. A comparative analysis of cell-cycle progression after exposure to pi mesons and cobalt gamma rays. Int. J. Radiat. Biol. 33, 1-10 (1978).

13. M. A. BENDER, Neutron induced genetic effects: A review. Radiat. Bot. 10, 225-247 (1970).

14. A. V. CARRANO, Induction of chromosomal aberrations in human lymphocytes by x rays and fission neutrons: Dependence on cell cycle stage. Radiat. Res. 63, 403-421 (1975).

15. S. WOLFE, Radiation genetics. In Mechanisms in Radiobiology, (M. Errera and A. Forssberg, Eds.), vol. I, pp. 419-475. Academic Press, New York, 1961.

16. R. J. M. FRY, A. G. GARCIA, K. H. ALLEN, A. SALLESE, T. N. TAHMISIAN, L. S. LOMBARD, and E. J. AINSWORTH, The effect of pituitary isografts on radiation carcinogenesis in the mammary and harderian glands of mice. In Biological Effects of Low Level Radiation Pertinent to Protection of Man and His Environment. Proceedings, IAEA, Chicago.

17. E. L. LLOYD, A. GEMMELL, C. B. HENNING, D. S. GEMMELL, and B. J. ZABRANSKY, Transformation of mouse embryo (C3H 10T 1/2) cells by alpha particles. Research Division Annual Report, July 1976-June 1977, Center for Human Radiobiology. Argonne National Laboratory Report 77-65, Argonne Illinois.

18. T.C.H. YANG, C. A. TOBIAS, E. A. BLAKELY, L. M. CRAISE, I. S. MADFES, C. PEREZ, and J. HOWARD, Cocarcinogenic effects of high-energy neon particles on the viral transformation of mouse C3H10T1/2 cells in vitro. Manuscript in preparation.

19. M. RICHOLD and P. D. HOLT, The effect of differing neutron energies on mutagenesis in cultured Chinese hamster cells. In Biological Effects of Neutron Irradiation. IAEA, Vienna, Austria, 1974.

20. R. COX, J. THACKER, and D. T. GOODHEAD, Inactivation and mutation of cultured mammalian cells by aluminum characteristic ultrasoft x rays. II. Dose-response of Chinese hamster and human diploid cells to aluminum x rays and radiations of different LET. Int. J. Radiat. Biol. 31, 561-567 (1977).

21. M. A. RITTER, J. E. CLEAVER, and C. A. TOBIAS, High-LET radiations induce a large proportion of non-rejoining DNA breaks. Nature 266, 653-655 (1977).

22. R. ROOTS, T.C.H. YANG, L. CRAISE, E. A. BLAKELY, and C. A. TOBIAS. Impaired repair capacity of DNA breaks induced in mammalian cellular DNA by accelerated heavy ions. Radiat. Res., in press.

23. G. W. BARENDSEN, C. J. KOOT, G. R. VAN KERSEN, D. K. BEWLEY, S. B. FIELD, and C. J. PARNELL, The effect of oxygen on impairment of the proliferative capacity of human cells in culture by ionizing radiations of different LET. Int. J. Radiat. Biol. 10, 317-327 (1966).

24. C. A. TOBIAS and P. W. TODD, Heavy charged particles in cancer therapy. In Radiobiology and Radiotherapy, U. S. National Cancer Monograph 24. National Cancer Institute, Bethesda, MD, 1967.

25. R. BIRD and J. BURKI, Survival of synchronized Chinese hamster cells exposed to radiation of different linear energy transfer. Int. J. Radiat. Biol. 27, 105-120 (1975).

26. E. J. HALL, R. P. BIRD, H. H. ROSSI, R. COFFEY, J. VARGA, and Y. M. LAM, Biophysical studies with high-energy argon ions. 2. Determinations of the relative biological effectiveness, the oxygen enhancement ratio, and the cell cycle response. Radiat. Res. 70, 469-479 (1977).

27. D. A. PHILBRICK, Radiation induced reproductive death as a function of mammalian cell ploidy. PhD Thesis, University of California, Berkeley, 1976.

28. J. M. FEOLA, C. RICHMAN, M. R. RAJU, S. B. CURTIS, and J. H. LAWRENCE, Effects of negative pions on the proliferative capacity of ascites tumor cells (lymphoma) in vivo. Radiat. Res. 34, 70-78 (1970).

29. C. LUCKE-HUHLE, E. A. BLAKELY, and C. A. TOBIAS, The influence of intercellular contact on mammalian cell survival after heavy-ion irradiation. European J. Cancer Suppl., in press.

30. S. B. CURTIS, T. S. TENFORDE, D. PARKS, W. A. SCHILLING, and J. T. LYMAN, Response of a rat rhabdomyosarcoma to neon and helium ion irradiation. Radiat. Res. 74, 274-288 (1978).

31. M. R. RAJU, E. BAIN, S. CARPENTER, R. A. COX, and J. B. ROBERTSON, Heavy particles in radiation therapy: A comparative study. 4. RBE and OER and the implications of this comparative study. Radiat. Res. 70, 672 (1977).

32. L. S. GOLDSTEIN, T. L. PHILLIPS, and K. K. FU, Biological effects of carbon and argon ions on tumor and normal tissues. Radiat. Res. 70, 671 (1977).

33. K. FU and T. PHILLIPS, The relative biological effectiveness and oxygen enhancement ratio of neon ions for the EMT6 tumor. Radiology 120, 439 (1976).

34. J. R. CASTRO and J. M. QUIVEY, Clinical experience and expectation with helium and heavy-ion irradiation. Int. J. Radiat. Oncol. Biol. Phys. 3, 127-132 (1977).

35. J. VAN DER VEEN, L. BOTS, and A. MES, Establishment of two human cell strains from kidney and reticule sarcoma of lung. Arch. Gesamte Virusforsch. 8, 230 (1958).

36. A. GHIORSO, H. GRUNDER, W. HARTSOUGH, G. LAMBERTSON, E. LOFGREN, K. LOU, R. MAIN, R. MOBLEY, R. MORGADO, W. SALSIG, and F. SELPH, The Bevalac: An economical facility for very high energetic heavy particle research. IEEE Trans. Nucl. Sci. NS-20, 155 (1973).

37. J. T. LYMAN, J. HOWARD, and A. A. WINDSOR, Heavy charged particle beam monitoring with segmented ionization chambers. Med. Phys. 2, 163 (1975).

38. J. T. LYMAN and J. HOWARD, Dosimetry and instrumentation for helium and heavy ions. Int. J. Radiat. Oncol. Biol. Phys. 3, 81-86 (1977).

39. C. A. TOBIAS, H. O. ANGER, and J. H. LAWRENCE, Radiological use of high-energy deuterons and alpha particles. Am. J. Roentgenol. Radium Ther. and Nucl. Med. 67, 1-27 (1952).

40. M. R. RAJU, J. T. LYMAN, T. BRUSTAD, and C. A. TOBIAS, Heavy charged particle beams. In Radiation Dosimetry (F. H. Attix, W. C. Roesch, and E. Tochilin, Eds.), vol. III, pp. 151-199. Academic Press, New York, 1966.

41. H. BICHSEL, Charged particle interactions. In Radiation Dosimetry, Vol. I: Fundamentals (F. H. Attix and W. C. Roesch, Eds.). New York, Academic Press, 1968.

42. R. H. THOMAS, J. T. LYMAN, and M. DE CASTRO, A mean estimate of the average energy required to create an ion pair in nitrogen by high-energy ions. Submitted to Radiat Res.

43. L. J. GOODMAN, $\overline{W}_N$ computed from recent measurements of $\overline{W}$ for charged particles. In Proceedings, Third Symposium of Neutron Dosimetry in Biology and Medicine, 23-27 May 1977 (G. Barger and E. G. Ebert, Eds.) p. 61. Brussels-Luxembourg, Commission of the European Communities, 1978.

44. L. J. GOODMAN and R. D. COLVETT, Biophysical studies with high-energy argon ions. I. Depth dose measurements in tissue equivalent liquid and in water. Radiat. Res. 40, 455-468 (1977)

45. G. P. STEWARD, Stopping power and range for any nucleus in the specific energy interval 0.01 to 500 MeV/amu in any nongaseous material. Lawrence Berkeley Laboratory Report UCRL-18127, 1968.

46. C. RICHARD-SERRE, Evaluation de la perte d'energie unitaire et du parcours pour des ions lourds de 10 MeV/nucleon jusqu'a 1000 MeV/nucleon. Laboratoire I. Division de la machine synchrocyclotron. CERN 72-19, 9 November 1972.

47. W. SCHIMMERLING, K. G. VOSBURGH, and P. W. TODD, Measurements of range in matter for relativistic heavy ions. Phys. Rev. B 7, 2895-2899 (1973).

48. H. L. BRADT and B. PETERS, The heavy nuclei of the primary cosmic radiation. Phys. Rev. 77, 35-70 (1950).

49. H. H. HECKMAN, D. E. GREINER, P. J. LINDSTROM, and F. S. BIESER, Fragmentation of nitrogen-14 nuclei at 2.1 GeV/nucleon. Science 174, 110 (1971).

50. H. D. MACCABEE and M. A. RITTER, Fragmentation of high-energy oxygen-ion beams in water. Radiat. Res. 60, 409 (1974).

51. W. SCHIMMERLING, D. ORTENDAHL, S. KAPLAN, G. GABOR, J. OZAWA, W. STEELE, and C. PEREZ-MENDEZ, Physical characterizations of heavy-ion beams. Radiat. Res. 74, 596 (1978).

52. A. CHATTERJEE, C. A. TOBIAS, and J. T. LYMAN, Nuclear fragmentation in therapeutic and diagnostic studies with heavy ions. Spallation Nuclear Reactions and Their Applications (B.S.P. Shen and M. Merker, Eds.) p. 169. Reidel Publishing Co., Dordrecht, Holland, 1976.

53. S. B. CURTIS, Calculated LET distributions of heavy-ion beams. Int. J. Radiat. Oncol. Biol. Phys. 3, 87-92 (1977).

54. J. D. CHAPMAN, J. STURROCK, J.W. BOAG, and J. O. CROOKALL, Factors affecting the oxygen tension around cells growing in plastic petri dishes. Int. J. Rad. Biol. 17, 305-328 (1970).

55. W. K. SINCLAIR, Radiobiological dosimetry. In Radiation Dosimetry (E. Tochilin, Ed.). Academic Press, New York, 1969.

56. M.S.S. MURTHY and A. R. LAKSHMANAN, Dose enhancement due to backscattered secondary electrons at the interface of two media. Radiat. Res. 67, 215-233 (1976).

57. D. E. LEA, Action of Radiations on Living Cells. Cambridge Univeristy Press, London and New York, 1955.

58. M. M. ELKIND and H. SUTTON, Radiation response of mammalian cells grown in culture. I. Repair of x-ray damage in surviving Chinese hamster cells. Radiat. Res. 13, 556-593 (1960).

59. R. WIDEROE, High-energy electron therapy and the two-component theory of radiation. Acta Radiol. 4, 257-278 (1966).

60. E. L. POWERS, J. T. LYMAN, and C. A. TOBIAS, Some effects of accelerated charged particles on bacterial spores. Int. J. Radiat. Biol. 14, 313-340 (1968).

61. B. S. JACOBSON, Evidence for recovery from x-ray damage in chlamydomonas. Radiat. Res. 7, 395-406 (1957).

62. W. K. SINCLAIR, The shape of radiation survival curves of mammalian cells cultured in vitro. In Biophysical Aspects of Radiation Quality. Technical Report, Series 58, pp. 21-43. IAEA, Vienna, 1966.

63. G. J. NEARY, Chromosome aberrations and the theory of RBE. I. general considerations. Int. J. Radiat. Biol. 9, 477-502 (1965).

64. A. M. KELLERER and H. H. ROSSI, The theory of dual radiation action. Curr. Topics Radiat. Res. Q. 8, 85-158 (1972).

65. A. M. KELLERER and H. H. ROSSI, A generalized formulation of dual radiation action. Radiat. Res. 75, 471-488 (1978).

66. K. H. CHADWICK and H. P. LEENHOUTS, A molecular theory of cell survival. Phys. Med. Biol. 18, 78-87 (1973).

67. K. H. CHADWICK and H. D. LEENHOUTS, The rejoining of DNA double-strand breaks and a model for the formation of chromosomal rearrangements. Int. J. Radiat. Biol. 33, 517-529 (1978).

68. R. H. HAYNES, The interpretation of microbial inactivation and recovery phenomena. Radiat. Res. Suppl. 6, 1-29 (1966).

69. A.E.S. GREEN and J. BURKI, A note on survival curves with shoulders. Radiat. Res. 60, 536-540 (1972).

70. D. M. GINSBERG and J. JAGGERS, Evidence that initial ultraviolet lethal damage in Escherichia coli strain XVT⁻A⁻U⁻ is independent of growth phase. J. Gen. Microbiol. 40, 171-184 (1965).

71. P. R. BEVINGTON, Data Reduction and Error Analysis for the Physical Sciences. McGraw Hill, New York, 1969.

72. P. TODD, J. P. GERACI, P. S. FURCENITTI, R. M. ROSSI, F. MIKAGE, R. B. THEUS, C. B. SCHROY, Comparison of the effects of various cyclotron-produced fast neutrons on the reproductive capacity of cultured human kidney (T-1) cells. Manuscript in preparation.

73. A. M. KELLERER, E. J. HALL, H. H. ROSSI, and P. TEEDLA, RBE as a function of neutron energy. II. Statistical analysis. Radiat. Res. 65, 172-186 (1976).

74. P. TODD, C. B. SCHROY, K. G. VOSBURGH, and W. SCHIMMERLING, Spatial distribution of a biological effect in a 3.9 GeV nitrogen-ion beam. Science 174, 1127-1128 (1971).

75. P. TODD, Radiobiology with heavy charged particles directed at radiotherapy. Europ. J. Cancer 10, 207-210 (1974).

76. E. J. HALL and S. LEHNERT, The biophysical properties of 3.9 GeV nitrogen ions. IV. OER and RBE determinations using cultured mammalian cells. Radiat. Res. 55, 431-436 (1973).

77. E. J. HALL and A. M. KELLERER, The biophysical properties of 3.9 GeV nitrogen ions. III. OER and RBE determinations using Vicia seedlings. Radiat. Res. 55 422-430 (1973).

78. R. ROISMAN, D. KALOFONOS, B. MARTINS, J. T. LYMAN, and C. A. TOBIAS, The effect of accelerated oxygen beams on human kidney cells. Radiat. Res. 59, 60 (1974).

79. C. A. TOBIAS, Pretherapeutic investigations with accelerated heavy ions. Radiology 108, 145-158 (1973).

80. D. KALOFONOS, Radiobiological oxygen effect and its relation to cancer therapy. M.S. Thesis, University of California, Berkeley, 1964.

81. J. B. ROBERTSON, J. R. WILLIAMS, R. A. SCHMIDT, J. B. LITTLE, D. F. FLYNN, and H. D. SUIT, Radiobiological studies of a high-energy modulated proton beam utilizing cultured mammalian cells. Cancer 35, 1664-1667 (1975).

82. M. R. RAJU, M. GNANAPURANI, B. MARTINS, J. HOWARD, and J. T. LYMAN, Measurement of OER and RBE of a 910 MeV helium ion beam using cultured cells (T-1). Radiology 162, 425 (1972).

83. M. R. RAJU, E. A. BLAKELY, J. HOWARD, J. T. LYMAN, D. P. KALOFONOS, B. MARTINS, and T.C.H. YANG, Human cell survival as a function of depth for a high-energy neon-ion beam. Radiat. Res 65, 191-194 (1976).

84. J. D. CHAPMAN, E. A. BLAKELY, K. C. SMITH, and R. C. URTASUN, Radiobiological characterization of the inactivating events produced in mammalian cells by helium and heavy ions. Int. J. Radiat. Oncol. Biol. Phys. 3, 97-102 (1977).

85. W. A. SCHILLING, S. B. CURTIS, T. S. TENFORDE, K. E. CRABTREE, S. J. DANIELS, J. HOWARD, and J. T. LYMAN, OER and RBE studies of the extended peaks of heavy-ion beams. Radiat. Res. 74, 587 (1978).

86. J. D. CHAPMAN, E. A. BLAKELY, K. C. SMITH, and R. C. URTASUN, Radiobiological characterization of the inactivating events produced in m mammalian cells by helium and heavy ions. Int. J. Radiat. Oncol. Biol. Phys. 3, 97-102 (1977).

87. H. H. ROSSI, A note on the effects of fractionation of high-LET radiation. Radiat. Res. 66, 170-173 (1976).

88. D. K. BEWLEY, A comparison of the response of mammalian cells to fast neutrons and charged particle beams. Radiat. Res. 34, 446-458 (1968).

89. J. E. TURNER and H. HOLLISTER, Relationship of the velocity of a charged particle to its relative biological effectiveness. Nature 207, 36-37 (1965).

90. R. KATZ, RBE, LET, and Z/β, Health Physics 18, 175 (1970).

91. S. B. CURTIS, The effect of track structure on OER at high LET. In Charged Particle Tracks in Solids and Liquids (G. E. Adams, D. K. Bewley, and J. W. BOAG, Eds.) pp. 140-142. Institute of Physics and the Physical Society, London, 1970.

92. R. KATZ, B. ACKERSON, M. HOMAYOONFAR, and S. C. SHARMA, Inactivation of cells by heavy-ion bombardment. Radiat. Res. 47, 402-425 (1971).

93. A. CHATTERJEE and C. A. TOBIAS, Relationships between track structure and heavy charged particles. In Radiobiological Experiments Using Accelerated Heavy Ions at the Bevatron. Lawrence Berkeley Laboratory Report LBL-2016, 1973.

94. A. CHATTERJEE and H. J. SCHAEFER, Microdosimetric structure of heavy ion tracks in tissue. Radiat. Environm. Biophys. 13, 215-227 (1976).

95. C. A. TOBIAS and A. CHATTERJEE, Relationships between track structure and biological effects of heavy charged particles. Radiat. Res. 55, 580-581 (1973).

96. C. A. TOBIAS, E. A. BLAKELY, F.Q.H. NGO, and A. CHATTERJEE, Repair-misrepair (RMR) model for the effect of single and fractionated doses of heavy accelerated ions. Radiat. Res. 74, 589 (1978).

U.S GPO:1979-689-058(F)7